

ADVANCED MATERIALS

Supporting Information

for *Adv. Mater.*, DOI 10.1002/adma.202407235

Open-Source Throttling of CD8⁺ T Cells in Brain with Low-Intensity Focused
Ultrasound-Guided Sequential Delivery of CXCL10, IL-2, and aPD-L1 for Glioblastoma
Immunotherapy

*Lei Dong, Yini Zhu, Haoge Zhang, Lin Gao, Zhiqi Zhang, Xiaoxuan Xu, Leqian Ying, Lu Zhang,
Yue Li, Zhengcheng Yun, Danqi Zhu, Chang Han, Tingting Xu, Hui Yang, Shenghong Ju*,
Xiaoyuan Chen*, Haijun Zhang* and Jinbing Xie**

Supporting Information

**Open-Source Throttling of CD8⁺ T Cells in Brain with Low-Intensity Focused
Ultrasound-Guided Sequential Delivery of CXCL10, IL-2, and aPD-L1 for
Glioblastoma Immunotherapy**

*Lei Dong, Yini Zhu, Haoge Zhang, Lin Gao, Zhiqi Zhang, Xiaoxuan Xu, Leqian Ying,
Lu Zhang, Yue Li, Zhengcheng Yun, Danqi Zhu, Chang Han, Tingting Xu, Hui Yang,
Shenghong Ju^{*}, Xiaoyuan Chen^{*}, Haijun Zhang^{*}, and Jinbing Xie^{*}*

Materials and Methods

Materials. Anti-mouse PD-L1 (B7-H1) was purchased from Bio X Cell (Cat. No. BE0101, New Hampshire, USA). The cytokine CXCL10 was obtained from GenScript Corporation (Z03587, Nanjing, China). Interleukin 2 (IL-2) was purchased from Sino Biological Inc. (11848-HNAE2, Beijing, China). Interleukin 4 (IL-4) and granulocyte-macrophage colony-stimulating factor (GM-CSF) were purchased from Pepro Tech (Pepro Tech, USA). The ester-capped polylactic acid glycolic acid copolymer PLGA75/25COOR with a molecular weight of 57,000 was purchased from Jinan Daigang Bioengineering Co. Ltd (DG-75DLG055, Jinan Daigang Biotechnology, China). Dipalmitoylphosphatidylcholine (DPPC) was purchased from AVT Pharmaceutical Tech Co., Ltd. (S01004, Shanghai, China). DSPE-PEG-1000 was purchased from Tanshtech (80010201-2000, Guangzhou, China). A specialized medium for CTLL-2 cells was purchased from Prosperity Life Sciences (CM-0331, Wuhan, China). CCK-8 kit was purchased from Beyotime Biotechnology (C0038, Shanghai, China). High glucose medium (DMEM), 1640 medium, 1% penicillin and streptomycin, and 0.25% trypsin-ethylenediaminetetraacetic acid (EDTA) were purchased from BioChannel Biological Technology Co., Ltd. (Nanjing, China). Meisen matrigel (MS0102ZY, Zhejiang Meisen Zhiyuan Biotechnology Co., Ltd. Fetal bovine serum was purchased in Umedium (3023A, Hefei, China). Lent-EF1a-P2A-luciferase-CMV-coGFP-P2A-Puro

lentivirus and polybrene were provided by Banma Biotechnology Co., Ltd. (Changsha, China). TNF- α (JM-02415M1; Jingmei Biological Technology, Nanjing) were purchased from Jiangsu Jingmei Biological Technology Co., Ltd. IFN- γ (JL10967; Jianglai biology, Shanghai) and IL-10 (JL20242; Jianglai biology, Shanghai). D-Luciferin potassium salt and Cy5-NHS were purchased from Nanjing Starleaf Biological Technology Co. ELISA was performed in triplicates as per the instructions of the manufacturer. All antibodies used for flow cytometry analysis were purchased from Dakewe Biotech Co. Analytical grades of all other chemicals were obtained from Sigma-Aldrich (Sigma-Aldrich, USA). GL261 Brain Cancer Mouse Tumor Antigen-Specific T Cell Assay Stimulation Kit was purchased from Absin Bioscience Inc (abs57014, Shanghai, China).

Cell culture. Mouse T-lymphocyte cell line CTLL-2, mouse dendritic cell line DC 2.4, mouse brain endothelial cell line bEnd.3, and mouse glioma cells GL261 were obtained from the Shanghai Institutes for Biological Sciences, Chinese Academy of Sciences. The cell lines tested negative for mycoplasma contamination and were regularly treated with mycoplasma removing agent (VivaCell, Shanghai, China). GL261 cells with stable luciferase expression (GL261-luc cells) were constructed in-house by Jiangsu Key Laboratory of Molecular and Functional Imaging. The bEnd.3, GL261 and GL261-luc cells were cultured and grown in high-sugar DMEM with 10% special grade fetal bovine serum FBS, DC2.4 cells were cultured and grown in RPMI-1640 medium with 10% special grade fetal bovine serum FBS, and the CTLL-2 cells were raised in CTLL-2-specific medium and incubated at 37°C in air, which containing 5% CO₂. These cells were suspended in serum-free cell cryopreservation solution (CELLSAVING, cat: C40100, New Cell&Molecular Biotech, China).

Animals. Female C57BL/6J mice (6-8 weeks, 20-22 g) were purchased from Jiangsu Huachuang Sino Pharma Tech Co., Ltd. Before performing experiments, all mice were maintained in a 12-h light-dark cycle with access to food and water. All animal experiments were performed in compliance with the relevant laws and approved by

the Institutional Animal Care and Use Committee of Southeast University School of Medicine (NO. 20220316049).

Extraction of DC cell membrane (DM). After continuously culturing DC2.4 in GM-CSF at a concentration of 10 ng/mL and IL-4 medium at 5 ng/mL for one week, the cells were stripped and collected with a cell scraper. The collected cells were then washed, twice with cooled PBS (pH=7.4). After that, the obtained cell precipitates were further suspended in hypotonic lysis buffer containing phenylmethylsulfonyl fluoride (PMSF) (Beyotime Institute of Biotechnology) and incubated in an ice bath for 15 min according to the manufacturer's instructions. Cells in the above solution were then broken 3 times using repeated freeze-thaw method and further centrifuged at 700*g for 10 min at 4°C. The supernatant was further centrifuged at 14,000*g for 30 minutes to collect the ruptured cell membranes. The cell membrane products were lyophilized and stored at -80°C. The lyophilized membrane material was rehydrated in ultrapure water before use. The protein content of the purified DM was assayed by BCA protein assay (KGP902, Nanjing KGI Biotechnology Co., Ltd., China).

Construction and characterization of IP@DCNBs, C@MBs. 0.125 g of PLGA and 200 µg of DM components were dissolved in 2.5 mL of CH₂Cl₂. 5 mg of aPD-L1 and 150 µg of IL-2 were dissolved in 0.375 mL of pre-cooled double-distilled water and added to the above dichloromethane solution. The W/O primary emulsion was emulsified by the ultrasonic cell disrupter for 2 min. 20 mL of W/O primary emulsion was poured into 20 mL of 1% PVA solution and continued to be emulsified for 1 min to form a W/O/W complex emulsion. Add 0.625 mL of isopropanol solution drop by drop to the complex emulsion and stir with a magnetic stirrer at room temperature for 4-6 h. Centrifuge at 12000 rpm for 10 min, discard the supernatant, collect the precipitate, and rinse with double-distilled water three times. The precipitates were washed three times with double-distilled water, stored at 80°C for 2-3 h, and freeze-dried for 24 h. The IP@DCNBs containing IL-2 and aPD-L1 were obtained.

14.41 mg DPPC and 7.017 mg DSPE-PEG-1000 were dissolved in 10 mL of

anhydrous ethanol and rotary evaporated at 48 °C to obtain a white film-like substance. Add 8 mL of double-distilled water, 1 mL of propylene glycol, and 1 mL of propanetriol, ultrasonic shaking at 50 °C to make the film fully dissolved in the hydrated solution, ultrasonic crushing (300w, 10min, on for 5s, off for 5s), closed. The membrane was divided into 10 aliquots, vacuumed, and filled with perfluoropropane gas, and 30 µg of cytokine CXCL10 was added to each aliquot. After shaking for 40 s, the C@MBs stock solution can be obtained. In addition, CXCL10 was further verified to be loaded by C@MBs by Dio labeling of DPPC, Cy5 labeling of CXCL10, and fluorescence microscopy. Surface morphology of C@MBs was characterized by atomic force microscope (AFM, Dimension Icon, Bruker, Billerica Massachusetts, United States; Tips model, Scan ASYST-Air).

aPD-L1, IL-2, and CXCL10 were labeled with Cy5 NHS (Cy5 NHS, 146368-14-1, Xi'an Rui Xi Biotechnology Co., Ltd., China). After purification, the encapsulation rate and loading of aPD-L1, IL-2, and CXCL10 in IP@DCNBs or C@MBs were calculated by a fluorescent microplate analyzer (Thermo Fisher Scientific, USA) using the following equations:

$$\text{encapsulation efficiency (\%)} = \frac{\text{amount of loaded drug}}{\text{amount of drug added}} * 100\%$$

$$\text{loading efficiency (\%)} = \frac{\text{amount of loaded drug}}{\text{amount of drug loaded nano vesicles}} * 100\%$$

Imaging was performed using a scanning electron microscope (SEM; Hitachi Regulus-8100, Hitachi High-Tech, Tokyo, Japan) and a transmission electron microscope (TEM; Hitachi HT-7800, Hitachi High-Tech, Tokyo, Japan). Hydration particle size potentials were obtained by dynamic light scattering (BeNano 1800 Zeta Pro, Dandong Bettersize™ Instruments Ltd., Dandong, China). A low-intensity focused ultrasound system (LIFU) was constructed by the Jiangsu Key Laboratory of Molecular and Functional Imaging. *In vivo*, imaging of microbubbles was evaluated using the CEUS with B-Mode mode of the Myriad Small Animal Ultrasound Imaging System (Mindray-ZS3, Shenzhen, China). A binocular Olympus light microscope (BX41-72H02, Tokyo, Japan) was used to observe the microbubble's external appearance and counting. The particle size changes of IP@DCNBs were detected

after LIFU with sound intensity of 0, 0.18, 0.40, 0.70, 1.1, 1.58, 2.15, 2.81, and 3.56 w/cm² was applied for 60 seconds. The change in particle size potential of C@MBs was detected after 60 seconds of LIFU action with sound intensity of 0, 0.18, 0.40, 0.70, 1.58, 2.81, and 3.56 w/cm². The counts and average diameters were measured every day for 7 days in three different solutions (pH 7.4 PBS, Dulbecco's modified Eagle medium (DMEM), and DMEM containing 10% fetal bovine serum (FBS)) to evaluate the stability of the IP@DCNBs or C@MBs.

***In vitro* and *in vivo* biosafety.** The safety of IP@DCNBs versus C@MBs on neural cell lines (PC12) was assessed using CCK-8 assay. Briefly, 5*10³ cells were added to each well of a 96-well plate treated with IP@DCNBs, C@MBs, and LIFU alone. After 48 h, the absorbance at 450 nm of each well was measured using a Multiskan FC zymograph (Thermo Fisher Scientific, USA) to indicate cell viability.

Hematoxylin-eosin (H&E) pathological staining and blood biochemical index assays were used to determine the biosafety of IP@DCNBs versus C@MBs. H&E staining was performed according to standard protocols (C0105S, Beyotime, China). Briefly, various nanopreparations were injected into mice through the tail vein (n=3), and different treatments were applied. 7 days later, blood was collected from the orbital sinus of mice, and then the mice were executed, and the internal organs (heart, liver, spleen, lungs, and kidneys) were collected for pathologic staining.

Evaluation of the chemotactic activity of CXCL10.

To evaluate the efficiency of LIFU-triggered C@MBs to release CXCL10, a 24-well migration chamber with 0.4 μm (3413, Unikon Biotechnology Co., Beijing, China). C@MBs were brought to the upper chamber, and the content of CXCL10 in the lower chamber was detected after 60 s of LIFU action at 0.40 w/cm². In this case, CXCL10 was labeled by Cy5, and the fluorescence signal of the lower chamber was observed by *IVIS* and quantified by a multifunctional enzyme marker. To test the ability of LIFU-triggered CXCL10 release from C@MBs to recruit T cells, a 24-well migration chamber (3421, Corning Incorporated, Corning, USA) with 4-μm pore size

chambers was used. Lymphocytes from the spleens of tumor-free C57BL/6J mice were obtained by lymphocyte isolation medium (P9000, Solarbio, China). GL261 cells (2×10^5 cells/mL, 1mL) were laid in the lower chamber. 600 μ L GL261 cell supernatant containing free CXCL10 (CXCL10=40 ng/mL), C@MBs and LIFU-C@MBs was placed in the lower chamber. The lower supernatant without CXCL10 was used as a control. In the upper chamber, 2×10^6 lymphocytes were plated, and after incubation at 37°C for 2 hours, lymphocytes migrating to the lower chamber were collected. Next, the cells were stained with anti-mouse CD3 (100302, BioLegend), CD45 (103112, BioLegend), CD8a (100708, BioLegend), and CD4 (100537, BioLegend) antibodies for 60 mins. Stained cells were then subjected to flow cytometry to analyze the proportion of CD3⁺CD4⁺ and CD3⁺CD8⁺ T cell populations. The number of lymphocytes was determined by CCK-8 assay. Next, *in vivo*, evaluation of LIFU combined with C@MBs open BBB was performed to recruit T cell effects. A suspension of 50 μ L of C@MBs was injected into the tail vein at a sound intensity of 0-2.81 w/cm² for 60 s. CXCL10 was labeled by Cy5, and an ultrasound intensity of 0-3.15 w/cm² was applied to LIFU for 60 s. Brain tissue homogenates were removed and quantified by an enzyme marker. Next, 10 μ L of 2% Evan's blue (EB) dye was injected into the tail vein. 2 h later, the brain was perfused and observed for the effect of opening the BBB. Similarly, Cy5 labeled CXCL10 was used to quantify CXCL10 in brain tissue by enzyme labeling, and the sound intensity was set at 0.40 w/cm² for 60 s. Brain homogenates were perfused and the CXCL10 was quantified in brain tissue by enzyme labeling. Tissue heart, liver, spleen, lung, kidney, and brain tumor distribution of CXCL10 was visualized by *IVIS* and quantified by fluorescence signal analysis. Meanwhile, lymphocytes from brain tissues were obtained by lymphocyte isolation medium (P9000, Solarbio, China). Brain tissues were stained with anti-mouse CD3 (100302, BioLegend), CD45 (103112, BioLegend), CD8a (100708, BioLegend), and CD4 (100537, BioLegend) antibodies for 60 mins. Stained cells were then subjected to flow cytometry to analyze the ratio of CD3⁺CD4⁺ and CD3⁺CD8⁺ T cell populations.

Tumor antigen-specific T-cell assay. GBM hormonal mice were subjected to four treatments of PBS, CXCL10, C@MBs, and LIFU combined with C@MBs, where the sound intensity of LIFU was 0.40 w/cm^2 . Tumor-infiltrating lymphocytes (TILs) were harvested from tumors by tumor dissociation kit (P9000, Solarbio, China). Further assessment of tumor antigen-specific T cells in tumor tissues was performed according to the protocol of GL261 Brain Cancer Mouse Tumor Antigen-Specific T Cell Detection Stimulation Kit (abs57014, Shanghai, China).

***In vitro* and *in vivo* T cell exhaustion assay.** To evaluate the efficiency of LIFU-triggered IP@DCNBs in releasing aPD-L1, a 24-well migration chamber with $0.2 \mu\text{m}$ (14311, LABSELECT, China) was used. The IP@DCNBs were brought to the upper chamber, and the aPD-L1 content in the lower chamber was detected after 1.58 w/cm^2 of LIFU action for 60 s. The aPD-L1 content in the lower chamber was measured by *IVIS*. In this case, aPD-L1 was labeled by Cy5, and the fluorescence signal of the lower chamber was observed by *IVIS* and quantified by a multifunctional enzyme marker. To test the ability of LIFU-triggered IL-2 released from IP@DCNBs to prevent T cell exhaustion, bEnd.3 cells (2×10^5 cells/mL, 1mL) were planted in 24-well migration chambers with $0.4 \mu\text{m}$ pore size of small chambers (14312, Labselect, China), and GL261-gfp cells (2×10^5 cells/ mL, 1mL) were laid in the lower chamber. 24h later, the chambers were done with four treatments of PBS, Positive control (Positive control, 50 ng/mL of IL-2 was added to the lower chamber), free IL-2, IP@DCNBs, and LIFU-conjugated IP@DCNBs (different treatments in the chambers corresponded to the concentration of IL-2 of 50 ng/mL). Cy5-labeled IL-2, the IL-2 in the lower chamber was quantified by using a fluorescent enzyme marker. After 96 h of treatment, all cells in the lower chamber were collected, and the cells were stained with anti-CD3 (100236, Biolegend, USA) for 90 min, and the stained cells were analyzed for the number of GL261-gfp and CTLL-2 by flow cytometry. CCK-8 was used to detect the cell viability of CTLL-2 and GL261-gfp, and the cell viability of GL261-gfp was detected by fluorescence microscopy (Japanese Olympus) to observe GL261-gfp survival. In addition, CTLL-2 cells were collected in the lower chamber

and western blotting (Wb) was performed to detect the expression of PD1, TIM-3, and CTLA-4 exhaustion indicators in CTLL-2 cells. CTLL-2 cells were stained with anti-mouse CD3 (100302, BioLegend), CD8a (100731, BioLegend), CD27 (135223, BioLegend), CD152 (106313, BioLegend) and CD366 (119703, BioLegend) antibodies staining for 60 mins. Stained cells were then subjected to flow cytometry to analyze the proportion of T-cell exhaustion.

***In vivo* pharmacokinetics of A2-MPC.** To investigate the pharmacokinetic behavior of native CXCL10, IL-2, aPD-L1, C@MBs, and IP@MBs (CXCL10, IL-2, or aPD-L1 labeled with Cy5), various nanoformulations were administrated into healthy SD rats via tail vein (n = 3). Then blood samples were collected at 1, 2, 4, 8, 12 and 24 h after injection of free CXCL10, IL-2, aPD-L1, C@MBs and IP@MBs. The serum was extracted and treated with an acid solution. Afterward, the concentrations of CXCL10, IL-2, or aPD-L1 were detected using the fluorescence microplate reader.

Parameters for safe and reversible open BBB. Male C57BL/6J mice (6-8 weeks, 20-22 g) were injected intravenously in the tail with a concentration of 1.4×10^7 /mL, 50 μ L of a suspension of C@MBs or IP@DCNBs, and the sound intensity of the LIFUs was set at 0-2.15 w/cm², with an action time duration of 60 s. Next, 10 μ L of a solution of evans blue (2% EB) was injected in the tail vein, and the perfusion was carried out 2 h later. The brain was taken. LIFU alone, LIFU combined with C@MBs, and LIFU combined with IP@DCNBs were observed to open the BBB region and extent. An equal amount of PBS buffer was injected into the tail vein of the control group. Meanwhile, to verify the reversibility of the opening of BBB by LIFU combined with C@MBs, as above, the sound intensity of LIFU was set to 0, 0.18, 0.4, or 0.70 w/cm², and, as above, after tail vein injection of C@MBs, 10 μ L of 2% EB solution was injected at the 0th, 3rd, 6th, and 12th h to observe the recovery of BBB. Then, to further find the relatively safe sound intensity interval for LIFU combined with C@MBs to open the BBB, H&E staining, TUNEL apoptosis assay, and immunofluorescence assay for inflammatory factors (IL-10, IL-6, IL-1 β , and TNF- α)

were performed on the brain tissue sections of the mice with brain tissue in the area of open BBB.

The delivery efficiency of aPD-L1. To further evaluate the efficiency of LIFU combined with IP@DCNBs to deliver aPD-L1, an *in vitro* model of BTB was constructed. The bEnd.3 cells (2×10^5 cells/ mL, 1mL) were planted in transwell chambers (24-well plate, PC membrane, 6.5 mm, pore size 0.4 μm) chambers of 24-well migration chamber (14312, Labselect, China). GL261 cells (1×10^5 cells/ mL, 1 mL) were spread in the lower chamber. Cy5-labeled aPD-L1 was subjected to four treatments, namely, PBS, aPD-L1, IP@DCNBs, and LIFU-IP@DCNBs (the sound intensity of the LIFU was set to 1.58 w/cm^2), respectively, in the chamber. Next, aPD-L1 in the lower chamber was quantified using a fluorescent enzyme marker. To assess the effect of LIFU-conjugated IP@DCNBs on the *in vitro* BTB model, recombinant Anti-ZO1 tight junction protein antibody (ab221547, Abcam, USA) and goat anti-rabbit IgG H&L (Alexa Fluor 488, Abcam, USA) were further used to stain the ZO-1 of bEnd.3 cells for the Tight junction proteins were immunofluorescently stained and visualized by fluorescence microscopy (Olympus, Japan). Meanwhile, to evaluate the efficiency of LIFU combined with C@MBs to deliver NBs. Did fluorescence labeling of NBs, five treatments of PBS, IP@NBs, IP@DCNBs, LIFU-C@MBs+IP@NBs, and LIFU-C@MBs+IP@DCNBs were performed, respectively (the sound intensity of LIFU was set to 0.40 w/cm^2). The delivery efficiency of NBs in brain tissues of the *in situ* GBM mouse model was assessed by zymography.

Mouse models and magnetic resonance imaging. Lent-EF1a-P2A-luciferase-CMV-coGFP-P2A-Puro lentivirus at a titer of 7×10^8 TU/mL was used to transfect GL261 cells at 50% fusion (MOI value of 100, polybrene concentration of 4 $\mu\text{g/mL}$ in the medium), and puromycin at a concentration of 3 $\mu\text{g/mL}$ screened for a GL261-luc cell line that stably expresses GFP and luciferase. A mixture of 4 μL matrix gel/PBS with 1×10^5 GL261 cells or GL261-luc cells was injected intracranially using a microliter syringe (Hamilton, USA) at coordinates of 0.5 mm anterior to the fontanelle, 1.5 mm

to the right, and 2 mm deep. MR imaging was performed using a 7.0 T MR small animal MR scanner (Bruker, Germany) and was confirmed by a T2-weighted imaging (T2WI) and fast spin-echo MR imaging sequence (repetition time/echo time, 2000/50 ms, matrix, 256*256, field of view, 20*20 mm, slice thickness, 1.0 mm) to monitor tumor growth). We used ImageJ (NIH, USA) to measure glioma-in-situ volume on T2WI images and to obtain the relative volume of glioma-in-situ versus the whole brain (relative tumor volume=glioma-in-situ volume/volume of the whole brain).

***In vivo* bioluminescence imaging.** Bioluminescence imaging was used to quantify tumor load in mice carrying GL261-luc. Tumor-bearing mice were injected with D-luciferin (150 mg/kg body weight, Starleaf Biological Technology Co., China), and images were taken using an animal live imaging system (ABL X5, Tanon, China). Data were subsequently analyzed using Living Image 2.5 software (Caliper Life Sciences, USA).

***In vivo* ultrasound imaging.** Male C57BL/6J mice (6-8 weeks, 20-22 g) were injected into the tail vein with 20 μ L of each of the three microbubble suspensions of Sonovue, C@MBs, or IP@DCNBs (all at a concentration of 1.4×10^7 /mL). Next, ultrasound images were generated using a commercially available ultrasound imaging device (ZS3; Myriad) in B-mode and contrast-enhanced ultrasound (CEUS) mode to record in situ imaging of the right lobe of the liver and gliomas in the brain corresponding to different time intervals. The ROI was analyzed by the Vevo Lab software, and the AUC values were obtained from the normalized raw data to output a baseline. A locally weighted scatterplot smoothing method was used to generate smooth infusion time curves.

***In vivo* biodistribution.** Near-infrared fluorescence (NIRF) imaging methods were used to assess the biodistribution of CXCL10 in the brains of an in situ glioma model mouse. First, C57BL/6J mice were subjected to four treatments of tail vein injection of PBS, free CXCL10, C@MBs, or LIFU-C@MBs (Cy5-labeled CXCL10, in which

the dosage of CXCL10 was 0.3 μ g per mouse), and the mice were scanned using an *IVIS* imaging system. 1h later, the mice were necropsied and the brain tissues were collected and washed with cold PBS, and cells were lysis buffer homogenization. Brain tissues were quantified in the free CXCL10, C@MBs, and LIFU-C@MBs groups using a fluorescent enzyme marker.

Next, 7 days after tumor implantation, free aPD-L1, IP@DCNBs, and LIFU-IP@DCNBs (Cy5 NHS-labeled aPD-L1) were injected through the tail vein of C57BL/6J mice with PBS. Mice were scanned at set time points (1h, 2h, 4h, 6h, 8h, 12h, 24h), and then mice were executed and organs (heart, liver, spleen, lungs, kidneys, and brain) were collected. The fluorescence signal of each organ was recorded using the *IVIS* imaging system. Next, the above organs were washed with cold PBS, weighed, and homogenized with cell lysis buffer. Finally, quantification of aPD-L1 biodistribution in the free aPD-L1, IP@DCNBs, and LIFU-IP@DCNBs groups was performed using a fluorescence enzyme marker.

To further investigate the deep delivery of aPD-L1 in different treatments, free aPD-L1, IP@DCNBs, and LIFU-IP@DCNBs were performed in GL261-carrying mice (aPD-L1 was labeled with Cy5), respectively. Mouse brain tissues were sequentially fixed with PBS (pH 7.4), 4% paraformaldehyde by transcardiac perfusion, extracted, sectioned, and stained with 4',6-diamidino-2-phenylindole (DAPI). Brain sections were observed with a fluorescence microscope (Olympus, Japan). The images were analyzed using Image-J software.

***In vivo* anti-tumor efficacy of in situ brain tumors.** GL261 cells or GL261-luc cells (1×10^5 cells) were intracranially inoculated at the same locations as above. The day of inoculation was day 0. On day 10 after inoculation with GL261 cells (or GL261-luc cells), mice were randomly assigned to receive, via the tail vein, aPD-L1, IL-2& aPD-L1, IP@NBs, IP@DCNBs, LIFU-IP@DCNBs, LIFU-C@MBs+LIFU-P@DCNBs and LIFU-C@MBs+LIFU-IP@DCNBs were treated at LIFU-IP@DCNBs (aPD-L1 at 1.5 mg/kg and 75 μ g/kg for both CXCL10 & IL-2) three times at two-day intervals. The treatment of LIFU-C@MBs+LIFU-IP@DCNBs was as follows: 5 min after

C@MBs injection, LIFU with an ultrasound intensity of 0.40 w/cm^2 was applied to the GBM region for a continuous period of 60 s. After 3 h, IP@DCNBs were injected into the circulation, and LIFU with an ultrasound intensity of 1.58 w/cm^2 was applied to the GBM region for a continuous period of 60 s. Tumor growth was monitored by MR scanning or bioluminescence imaging every 5 days from day 0 to day 20. The body weight of the mice was also monitored at the same time point. Mouse survival was calculated and statistical significance was determined using the log-rank test.

Brain tissues were obtained and fixed with 4% paraformaldehyde, and then sequentially dehydrated in a graded concentration of alcohol solution. After embedding in paraffin, gliomas were sectioned according to the manufacturer's protocol. Tumors were detected with PCNA (abs100392, Absin, Shanghai, China) and Ki67 (ab15580, Abcam, Inc., USA) antibodies and immunofluorescence detection kits (SangonBiotech, Co., Ltd., Shanghai, China) and TUNEL detection kits (BeyotimeBiotech. Shanghai, China) were used to desorb and rehydrate the tumor sections, followed by immunofluorescence staining. Images were analyzed using Image-J software.

Immunosuppressive environment analysis. Tumor levels of IFN- γ , IL-10, TGF- β , and TNF- α were measured using the corresponding Elisa kits (MM-0182M1, MM-0176M1, MM-0689M1, MM-0132M1, Jiangsu Enzyme Immunity Industry Co., Ltd, China). Tumor tissues were harvested, homogenized, and then centrifuged. The supernatant was aliquoted and diluted with Elisa assay buffer according to the manufacturer's instructions. Immunofluorescence sections of tumor tissues from different treatment groups were quadruple labeled (CD45, CD3, CD8, DAPI labeled nuclei).

For T-cell analysis, $0.5 \mu\text{g/ mL}$ Collagenase D (Roche, Basel, Switzerland), $0.5 \mu\text{g/ mL}$ DNase1 (Vazyme Biotec Co., Ltd, China), and $3 \mu\text{g/mL}$ DNase1 (Sigma Aldrich, USA) were used. Brain infiltrating immune cells were then isolated with a lymphocyte isolation solution (17-5442-03, GE, USA). The cells were then stained with anti-CD45, anti-CD3, anti-CD4, anti-CD8a, anti-CD25 (103112, 100203,

100537, 100707, 102015, Biolegend, USA) and anti-Foxp3 antibodies (126403, Biolegend, USA) for 90 min. Foxp3 staining was performed according to the Biolegend intracellular staining protocol (424401, Biolegend, USA). Thereafter, flow cytometry was performed on the stained cells to analyze the CD8⁺ and Foxp3⁺ T cell populations (2*10⁴ events were collected for analysis). In addition, tumor tissues of different treatment groups were immunofluorescence sectioned for quadruple labeling (CD4, CD25, Foxp3, DAPI-labeled nuclei).

To further assess the effect of delayed T cell exhaustion *in vivo*, tumor tissues from different treatment groups were immunofluorescently sectioned for quadruple labeling (CD3, PD1, TIM-3, and CTLA-4, DAPI labeled nuclei). They were also stained with anti-CD45, anti-CD3, anti-CD4, anti-CD8a, anti-PD1, anti-TIM-3 and anti-CTLA-4 (Biolegend, USA). Thereafter, the stained cells were analyzed by flow cytometry (2*10⁴ events were collected for analysis).

To further analyze the memory T cells, 45 days after inoculation, five mice treated with LIFU-C@MBs+LIFU-IP@DCNBs were randomly selected. Next, spleen cells were taken and stained with anti-mouse CD45, CD3, CD8a, CD44 (103112, 100203, 100707, 103029, Biolegend, USA) and CD62L antibodies (104427, Biolegend, USA). Thereafter, the stained cells were analyzed by flow cytometry (2*10⁴ events were collected for analysis).

For tumor re-challenge studies, C57BL/6J mice were re-injected with 1*10⁵ GL261 cells 45 days after the first pick-up and subsequently treated with LIFU-C@MBs+LIFU-IP@DCNBs. Simultaneous MR imaging was performed to monitor tumor size and to record survival time.

Statistics Analysis. Before analysis, the raw data were tested for normality and homogeneity of variances using Kolmogorov-Smirnov and Levene's tests, respectively, and the data were transformed where necessary. One-way analysis of variance (ANOVA) followed by Tukey's honest significant difference (HSD) post hoc test was used to evaluate the differences of CD8⁺ T cell ratio, antibody activity, tumor volume, body weight, inflammatory cytokine level, and data in western blotting,

immunostaining, and flow cytometry analysis after various treatments. If the variance is not unequal, then the rank sum test was used. The independent sample t-test was performed to analyze and compare the tumor volume in the rechallenge study and memory T cell ratio in immune memory analysis. Statistical analysis of overall survival time was performed using log-rank tests. A p-value < 0.05 was considered statistically significant. All statistical tests were performed using SPSS software (SPSS version 19.0, SPSS Inc., USA) and data were reported as standard deviation \pm mean (S. D.). The significance is expressed as * p < 0.05, ** p < 0.01, *** p < 0.001 relative to control group; # p < 0.05, ## p < 0.01, and, ### p < 0.001 relative to all groups; ns: no significance.

	aPD-L1(15mg/125mg)	IL-2(150µg/125mg)	CXCL10(30µg/1mL)
Encapsulation efficiency (%)	62.581 ± 1.68	95.385 ± 3.808	96.142 ± 1.82
Loading efficiency (%)	7.509 ± 0.201	0.087 ± 0.003	1.328 ± 0.025

Table S1. Loading efficiency (%) and encapsulation efficiency (%) of CXCL10, IL-2 and aPD-L1 (n=3).

Time/1d	WBC(10 ⁹ /L)	RBC(10 ¹² /L)	HGB(g/L)	PLT(10 ⁹ /L)	Gran(10 ⁹ /L)	Lym(10 ⁹ /L)	Mon(10 ⁹ /L)
Control	5.83±1.13	8.11±0.61	144±6.53	1101±137.59	2.09±0.82	3.82±0.48	0.46±0.19
aPD-L1	5.86±0.45	8.10±0.32	137±3.26	1196±137.75	2.39±0.72	3.82±0.51	0.61±0.22
IP	4.60±0.17	6.86±0.36	119.22±6.47	978±50.59	1.64±0.02	3.11±0.13	0.41±0.01
IP@NBs	3.8±0.19	8.26±0.32	143.85±6.58	771±78.73	0.85±0.21	3.11±0.19	0.55±0.21
IP@DCNBs	4.09±0.20	7.45±0.29	129.40±5.91	823±38.29	1.38±0.20	2.8±0.19	0.47±0.21
LIFU-C@MBs+ IP@DCNBs	4.5±0.21	8.17±0.31	140.96±6.45	740±33.67	1.63±0.20	3.07±0.19	0.47±0.21
LIFU-C@MBs+ LIFU-P@DCNBs	4.14±0.20	6.85±0.19	117.76±4.38	544±111.09	0.84±0.19	3.35±0.19	0.57±0.21
LIFU-C@MBs+ LIFU-IP@DCNBs	5.60±0.23	7.10±0.28	118.80±5.21	611±28.39	1.17±0.20	4.40±0.19	0.65±0.21
Reference range	1.05-10.60	6.50-11.50	110-165	400-2300	0.62-7.60	0.90-10.60	0.04-1.40

Time/3d	WBC(10 ⁹ /L)	RBC(10 ¹² /L)	HGB(g/L)	PLT(10 ⁹ /L)	Gran(10 ⁹ /L)	Lym(10 ⁹ /L)	Mon(10 ⁹ /L)
Control	5.28±0.28	8.68±0.46	151.67±8	2019±106.56	1.43±0.07	3.46±0.18	0.38±0.02
aPD-L1	5.15±0.36	7.97±0.56	141.01±9.85	1038±72.53	1.6±0.11	3.32±0.23	0.24±0.02
IP	4.22±0.11	7.15±0.23	121.54±3.49	1207±29.2	1.11±0.02	2.87±0.09	0.26±0.01
IP@NBs	3.44±0.09	7.44±0.2	137.49±3.67	590±15.77	0.51±0.01	2.7±0.07	0.23±0.01
IP@DCNBs	3.79±0.1	7.07±0.19	128.45±3.43	847±22.66	1.11±0.03	2.5±0.07	0.18±0.02
LIFU-C@MBs+ IP@DCNBs	4.39±0.12	7.99±0.21	142.5±3.81	799±21.37	1.3±0.04	2.91±0.08	0.17±0.01
LIFU-C@MBs+ LIFU-P@DCNBs	3.82±0.1	6.42±0.17	117.41±3.14	574±15.34	0.92±0.02	3±0.08	0.3±0.02
LIFU-C@MBs+ LIFU-IP@DCNBs	5.18±0.14	6.91±0.18	121.43±3.24	559±14.96	0.81±0.02	3.88±0.11	0.48±0.03
Reference range	1.05-10.60	6.50-11.50	110-165	400-2300	0.62-7.60	0.90-10.60	0.04-1.40

Time/7d	WBC(10 ⁹ /L)	RBC(10 ¹² /L)	HGB(g/L)	PLT(10 ⁹ /L)	Gran(10 ⁹ /L)	Lym(10 ⁹ /L)	Mon(10 ⁹ /L)
Control	4.83±0.13	8±0.21	141.5±3.78	936.3±25.02	1.28±0.04	3.23±0.09	0.31±0.01
aPD-L1	5.09±0.14	7.81±0.21	138.49±3.7	997.51±26.65	1.5±0.04	3.32±0.09	0.27±0.01
IP	4.04±0.11	6.72±0.21	116.83±3.49	859.53±30.17	1.09±0.03	2.78±0.09	0.25±0.01
IP@NBs	3.63±0.1	8.33±0.23	142.5±3.81	816.88±21.83	0.78±0.02	2.84±0.08	0.21±0.01
IP@DCNBs	3.96±0.11	7.57±0.2	134.47±3.59	824.91±22.04	1.13±0.03	2.66±0.07	0.17±0.02
LIFU-C@MBs+ IP@DCNBs	4.47±0.12	8.02±0.21	144.51±3.86	768.71±20.54	1.31±0.04	2.95±0.08	0.2±0.01
LIFU-C@MBs+ LIFU-P@DCNBs	3.98±0.11	8.53±0.23	134.47±3.59	498.76±13.33	1.6±0.04	3.13±0.09	0.26±0.02
LIFU-C@MBs+ LIFU-IP@DCNBs	5.26±0.14	8.93±0.24	120.42±3.22	588.07±15.71	2.8±0.08	3.95±0.11	0.51±0.01
Reference range	1.05-10.60	6.50-11.50	110-165	400-2300	0.62-7.60	0.90-10.60	0.04-1.40

Table S2. Hematological parameters after treatment with various nano-formulations (n=3).

Time/1d	ALT(u/L)	AST(u/L)	TBIL(μ mol/L)	Crea(μ mol/L)	Urea(mmol/L)	UA(mmol/L)
Control	35.164 \pm 1.343	38.08 \pm 1.379	29.785 \pm 1.276	141.837 \pm 2.039	31.97 \pm 0.501	0.378 \pm 0.004
aPD-L1	41.636 \pm 5.153	33.486 \pm 3.593	30.396 \pm 2.788	120.877 \pm 1.827	35.786 \pm 0.456	0.333 \pm 0.014
IP	35.068 \pm 1.513	35.896 \pm 1.168	32.733 \pm 2.347	109.395 \pm 1.711	37.375 \pm 0.314	0.339 \pm 0.017
IP@NBs	37.007 \pm 3.535	37.177 \pm 1.12	35.023 \pm 1.166	138.867 \pm 2.009	41.034 \pm 0.766	0.347 \pm 0.009
IP@DCNBs	37.085 \pm 4.483	38.598 \pm 0.834	32.884 \pm 1.546	136.2 \pm 1.982	40.454 \pm 0.265	0.35 \pm 0.025
LIFU-C@MBs+						
IP@DCNBs	35.973 \pm 1.353	34.598 \pm 3.195	32.614 \pm 1.562	102.569 \pm 1.642	42.128 \pm 1.107	0.347 \pm 0.02
LIFU-C@MBs+						
LIFU-P@DCNBs	38.942 \pm 0.925	35.228 \pm 4.06	33.765 \pm 0.813	118.022 \pm 1.798	36.603 \pm 0.571	0.348 \pm 0.013
LIFU-C@MBs+						
LIFU-IP@DCNBs	43.174 \pm 3.353	35.52 \pm 0.988	33.915 \pm 2.132	124.131 \pm 1.86	33.806 \pm 0.988	0.336 \pm 0.022
Reference range	33-49	29-43	25.7-39.5	99.8-150	6.15-8.33	0.30-0.39

Time/3d	ALT(u/L)	AST(u/L)	TBIL(μ mol/L)	Crea(μ mol/L)	Urea(mmol/L)	UA(mmol/L)
Control	39.312 \pm 1.797	37.739 \pm 2.764	36.601 \pm 1.558	134.093 \pm 10.261	7.895 \pm 0.09	0.346 \pm 0.023
aPD-L1	38.572 \pm 3.279	39.086 \pm 3.602	34.941 \pm 1.75	145.032 \pm 4.767	6.357 \pm 0.135	0.355 \pm 0.014
IP	39.544 \pm 3.93	39.657 \pm 1.594	32.258 \pm 2.194	131.736 \pm 10.022	6.519 \pm 0.213	0.351 \pm 0.023
IP@NBs	41.488 \pm 4.249	40.494 \pm 0.227	30.453 \pm 1.495	132.462 \pm 1.597	6.406 \pm 0.05	0.358 \pm 0.017
IP@DCNBs	40.131 \pm 2.488	39.532 \pm 1.495	32.174 \pm 2.312	126.638 \pm 10.831	6.304 \pm 0.042	0.334 \pm 0.036
LIFU-C@MBs+						
IP@DCNBs	38.147 \pm 1.518	36.323 \pm 2.62	35.015 \pm 2.093	117.011 \pm 7.801	6.55 \pm 0.272	0.341 \pm 0.031
LIFU-C@MBs+						
LIFU-P@DCNBs	41.608 \pm 1.718	36.374 \pm 2.674	36.596 \pm 1.474	133.202 \pm 6.79	6.78 \pm 0.708	0.344 \pm 0.031
LIFU-C@MBs+						
LIFU-IP@DCNBs	41.475 \pm 3.924	39.696 \pm 2.065	34.549 \pm 1.555	136.924 \pm 2.708	6.582 \pm 0.196	0.354 \pm 0.013
Reference range	33-49	29-43	25.7-39.5	99.8-150	6.15-8.33	0.30-0.39

Time/7d	ALT(u/L)	AST(u/L)	TBIL(μ mol/L)	Crea(μ mol/L)	Urea(mmol/L)	UA(mmol/L)
Control	38.423 \pm 2.572	37.798 \pm 2.763	37.334 \pm 1.201	126.249 \pm 11.541	7.715 \pm 0.237	0.347 \pm 0.023
aPD-L1	40.225 \pm 1.853	39.476 \pm 3.705	35.229 \pm 1.344	138.341 \pm 9.106	6.49 \pm 0.303	0.358 \pm 0.013
IP	40.882 \pm 2.708	39.836 \pm 1.464	32.028 \pm 2.508	132.891 \pm 9.161	6.638 \pm 0.069	0.352 \pm 0.022
IP@NBs	42.036 \pm 4.982	41.073 \pm 1.046	30.123 \pm 1.903	134.748 \pm 1.843	6.538 \pm 0.237	0.363 \pm 0.021
IP@DCNBs	40.581 \pm 1.925	39.57 \pm 1.443	32.324 \pm 2.286	126.862 \pm 10.65	6.43 \pm 0.218	0.339 \pm 0.032
LIFU-C@MBs+						
IP@DCNBs	38.066 \pm 1.63	39.535 \pm 2.465	35.597 \pm 2.049	116.008 \pm 8.746	6.666 \pm 0.111	0.317 \pm 0.015
LIFU-C@MBs+						
LIFU-P@DCNBs	41.082 \pm 2.157	39.587 \pm 2.464	37.244 \pm 0.726	134.976 \pm 5.583	6.904 \pm 0.648	0.335 \pm 0.019
LIFU-C@MBs+						
LIFU-IP@DCNBs	41.242 \pm 3.888	39.633 \pm 2.151	34.94 \pm 1.262	139.795 \pm 2.587	6.73 \pm 0.374	0.359 \pm 0.018
Reference range	33-49	29-43	25.7-39.5	99.8-150	6.15-8.33	0.30-0.39

Table S3. Biochemical parameters after treatment with various nano-formulations (n=3).

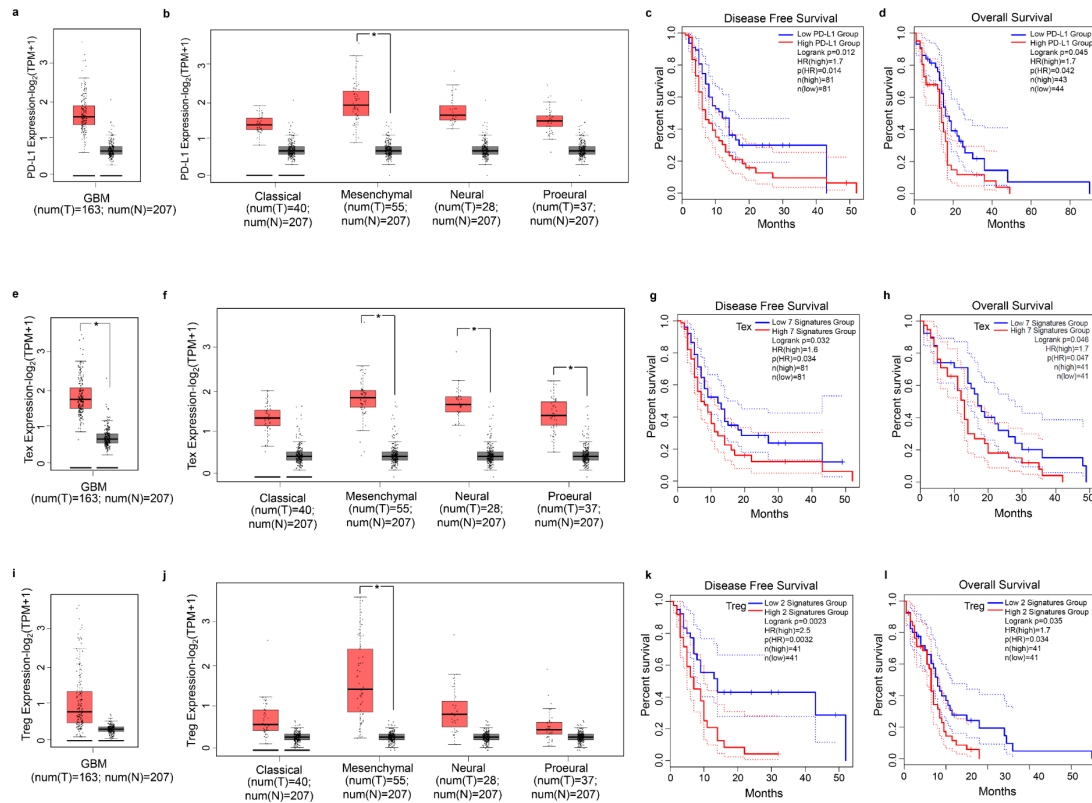


Figure S1. Association between immune components and prognosis in patients with GBM. Mining for information in the TCGA, and GTEx databases via <http://gepia2.cancer-pku.cn/>. a, b, c, d) Expression of PD-L1 gene was significantly increased ($*p < 0.05$) in Mesenchymal GBM subtypes compared to normal subjects. In GBM, patients with low expression of PD-L1 had significantly higher recurrence survival and overall survival than patients with high expression of PD-L1. e, f, g, h) Expression of Tex-related gene set (HAVCR2, TIGIT, LAG3, PDCD1, CXCL13, LAYN, TIM3, CTLA4) was significantly increased in GBM patients compared to normal subjects ($*p < 0.05$). In GBM, patients with low expression of the Tex-related gene set had significantly higher recurrence survival and overall survival than patients with high expression of the Tex-related gene set. i, j, k, l) Expression of the Treg-specific gene set (FOXP3-IL2RA), was significantly increased in Mesenchymal GBM subtypes compared to normal subjects ($*p < 0.05$). In GBM, patients with low expression of the Treg-related gene set had significantly higher recurrence survival and overall survival than those with high expression of the Treg-related gene set.

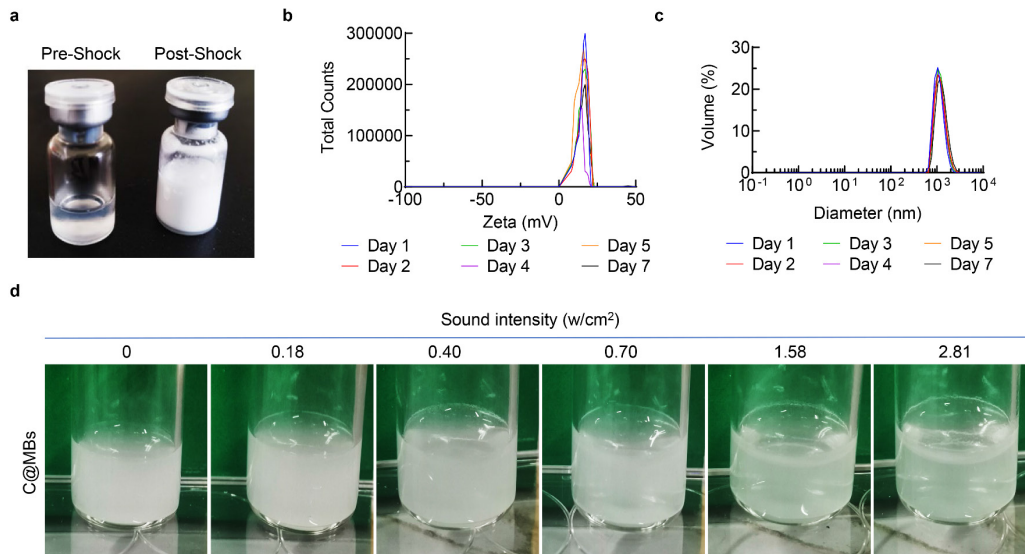


Figure S2. Changes in particle size and potential after C@MBs with ultrasound treatment. a) White microbubble suspension formed after 45 s of shaking of C@MBs stock solution. C@MBs were resuspended in pH 7.4 PBS for 7 days (n=3). b, c) 7-day particle size potential changes of C@MBs and observation of suspension translucency (n=3). d) C@MBs were resuspended in PBS (pH = 7.4).

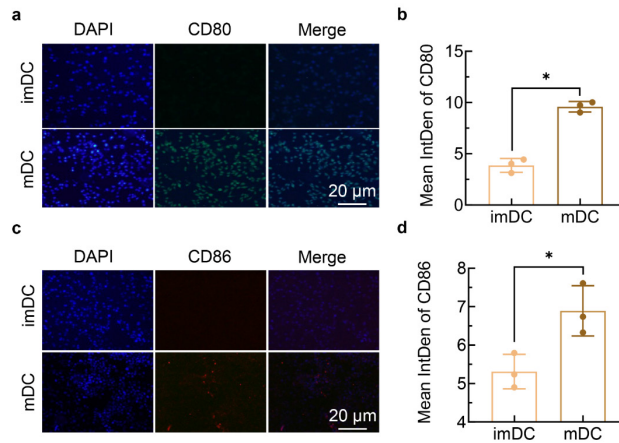


Figure S3. Immunofluorescence labeling of CD80 & CD86 molecules expressed by imDC cells and mDC cells. Where Alexa Fluor® 488 was labeled CD80 and Alexa Fluor® 647 was labeled CD86. b, d) Quantification of CD80 and CD86 expressed by imDC cells and mDC cells (5 ng/ml IL-4 with 10 ng/ml GM-CSF prompted the transformation of imDC cells into mDC cells, n=3). Data are expressed as mean \pm standard deviation. Statistical significance was calculated by one-way ANOVA with the Tukey post hoc test. * $p < 0.05$.

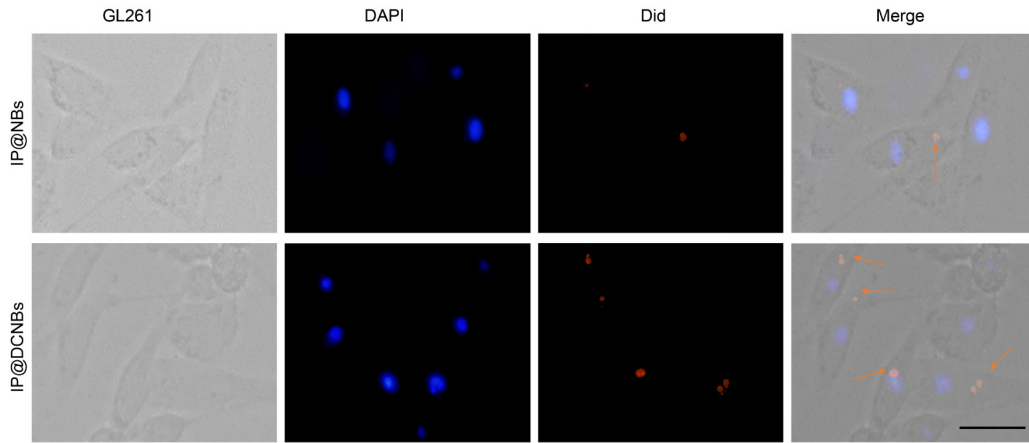


Figure S4. IP@DCNBs converge towards tumor cells. Fluorescence microscopy to observe the uptake of Did-labeled IP@DCNBs or IP@NBs by GL261 cells. Scale bar=10 nm.

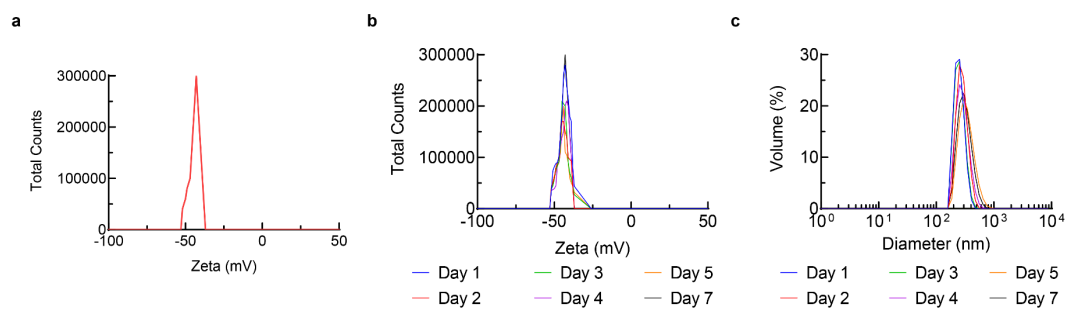


Figure S5. Seven-day changes in particle size and potential of IP@DCNBs. a) The average IP@DCNBs potential was -41.47 ± 0.95 mV. b, c) 7-day average potential and particle size changes of IP@DCNBs resuspended in pH 7.4 PBS (n=3).

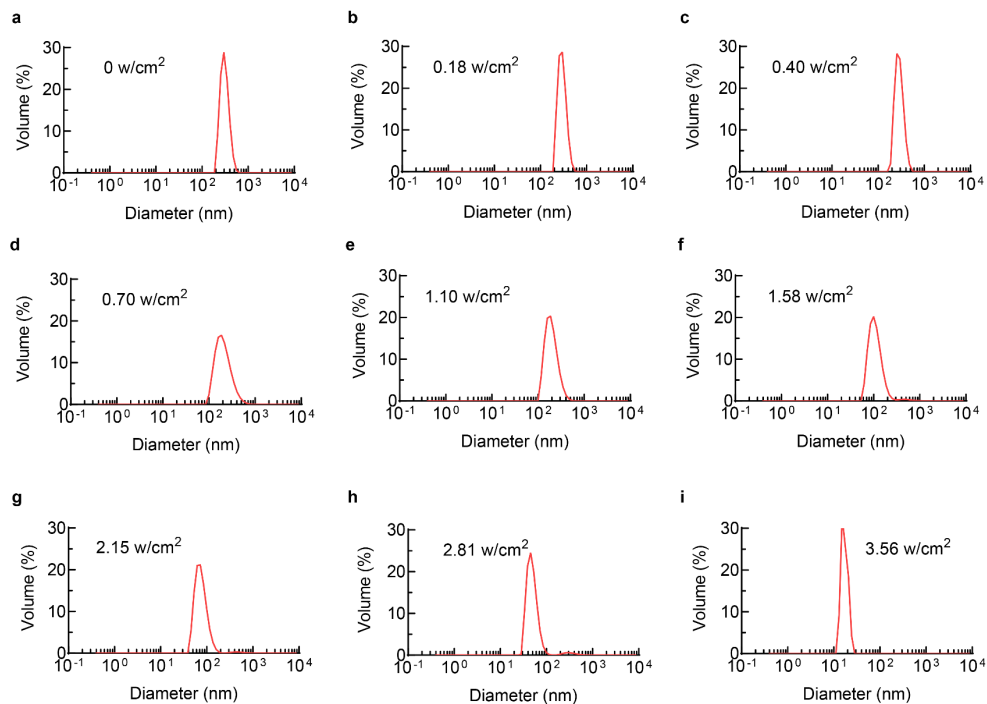


Figure S6. Changes in particle size of IP@DCNBs after LIFU action with different sound intensities. The particle size distributions of IP@DCNBs were 371.3, 281.0, 249.5, 189.1, 124.0, 96.80, 86.23, 49.92, and 23.72 nm as detected by Malvern particle sizer after 60 s of sustained action at sound intensities of 0.18, 0.40, 0.70, 1.10, 1.58, 2.15, 2.81 and 3.56 w/cm².

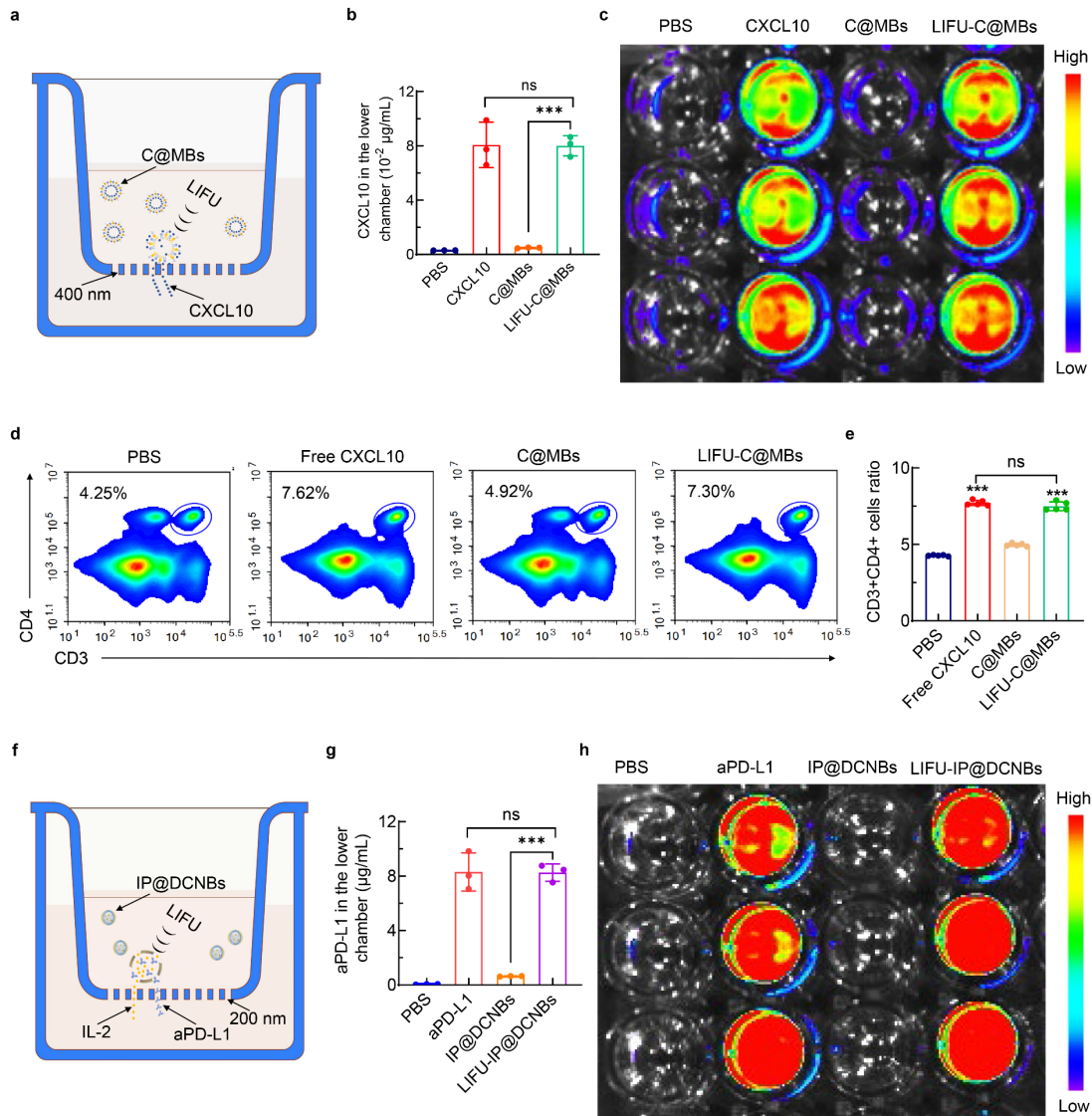


Figure S7. LIFU-triggered drug release efficiency. a, b, c) CXCL10 was labeled by Cy5, and the luminescence was quantified using a microplate reader. The efficiency of CXCL10 release from LIFU-triggered C@MBs with a sound intensity of 0.40 w/cm² was evaluated by *IVIS* (n=3). d, e) Ultrasound intensity was set at 0.40 w/cm² and flow quantification of the proportion of CD4⁺ T cells recruited after LIFU combined with C@MBs open BBB (n=5). f, g, h) The efficiency of LIFU-triggered IP@DCNBs to release IL-2 and aPD-L1 with a sound intensity of 1.58 w/cm² was evaluated by *IVIS*. IL-2 or aPD-L1 was labeled by Cy5, and the luminescence was quantified using a microplate reader (n=3). Data are expressed as mean ± standard deviation. Statistical significance was calculated by one-way ANOVA with the Tukey post hoc test. ****p* < 0.001, ns: no significance.

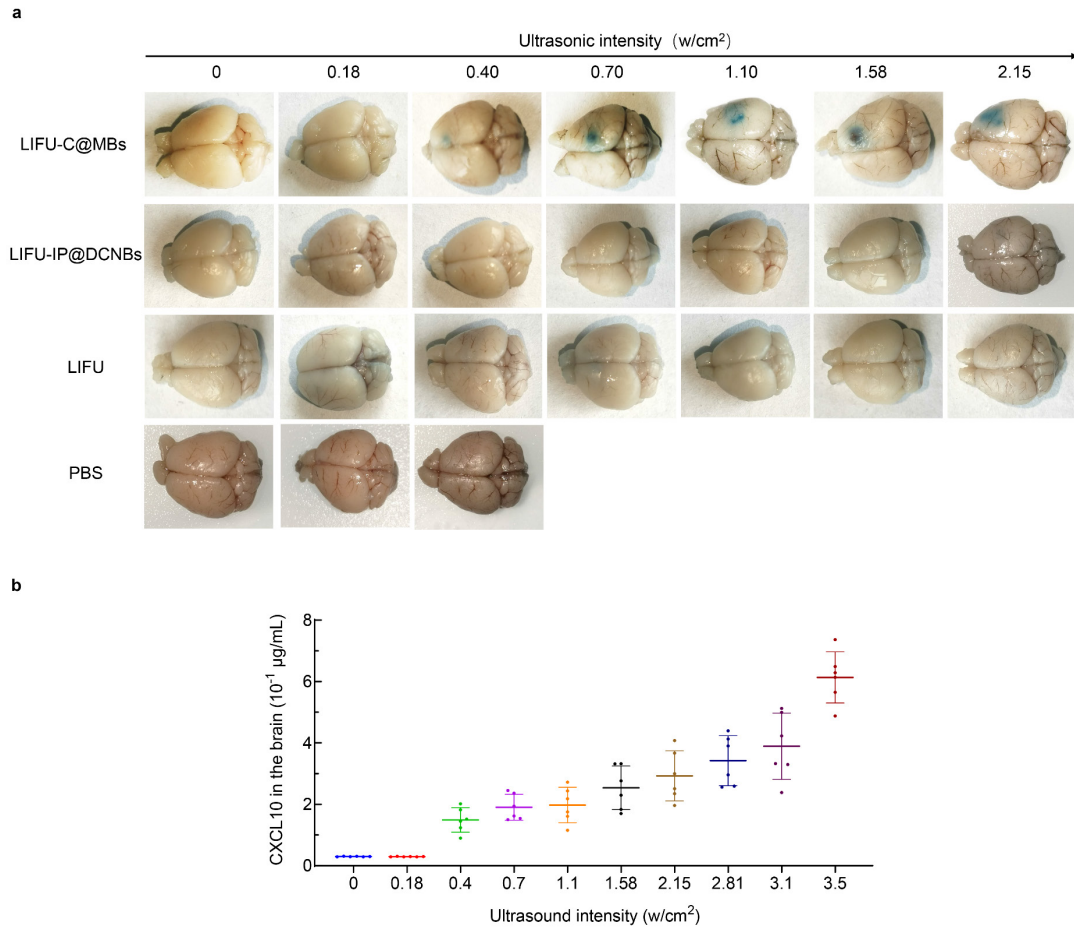


Figure S8. Opening of the BBB *in vivo*. Equal amounts of C@MBs and IP@DCNBs combined with LIFUs of different sound intensities and LIFU alone acted for 60 s. The area and degree of BBB opening were determined by injecting and observing the penetration of 2% EB dye. Quantification of CXCL10 in brain tissue by zymography, Cy5-labeled CXCL10.

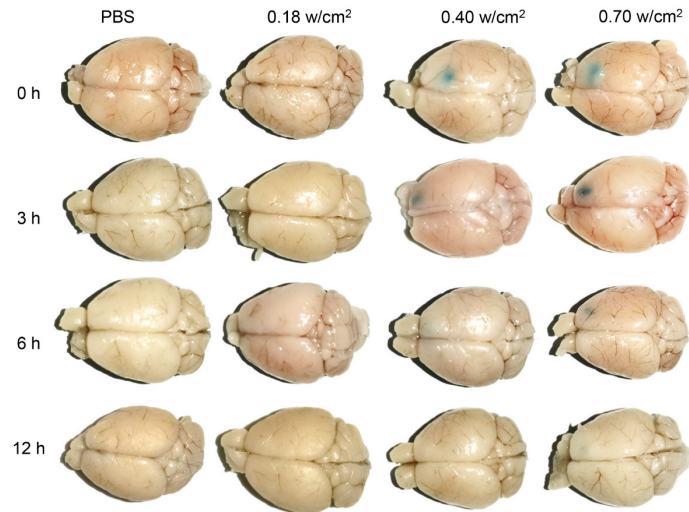


Figure S9. LIFU combined with C@MBs to open up BBB reversibility. Intravenous injection of 20 μL of C@MBs suspension (concentration of $7.5 \times 10^5/\text{ml}$) with sound intensity of 0.18, 0.40, and 0.70 w/cm^2 acted for 60 s, followed by intravenous injection of 20 μL of 2% EB solution at 0, 3, 6 and 12 h, respectively.

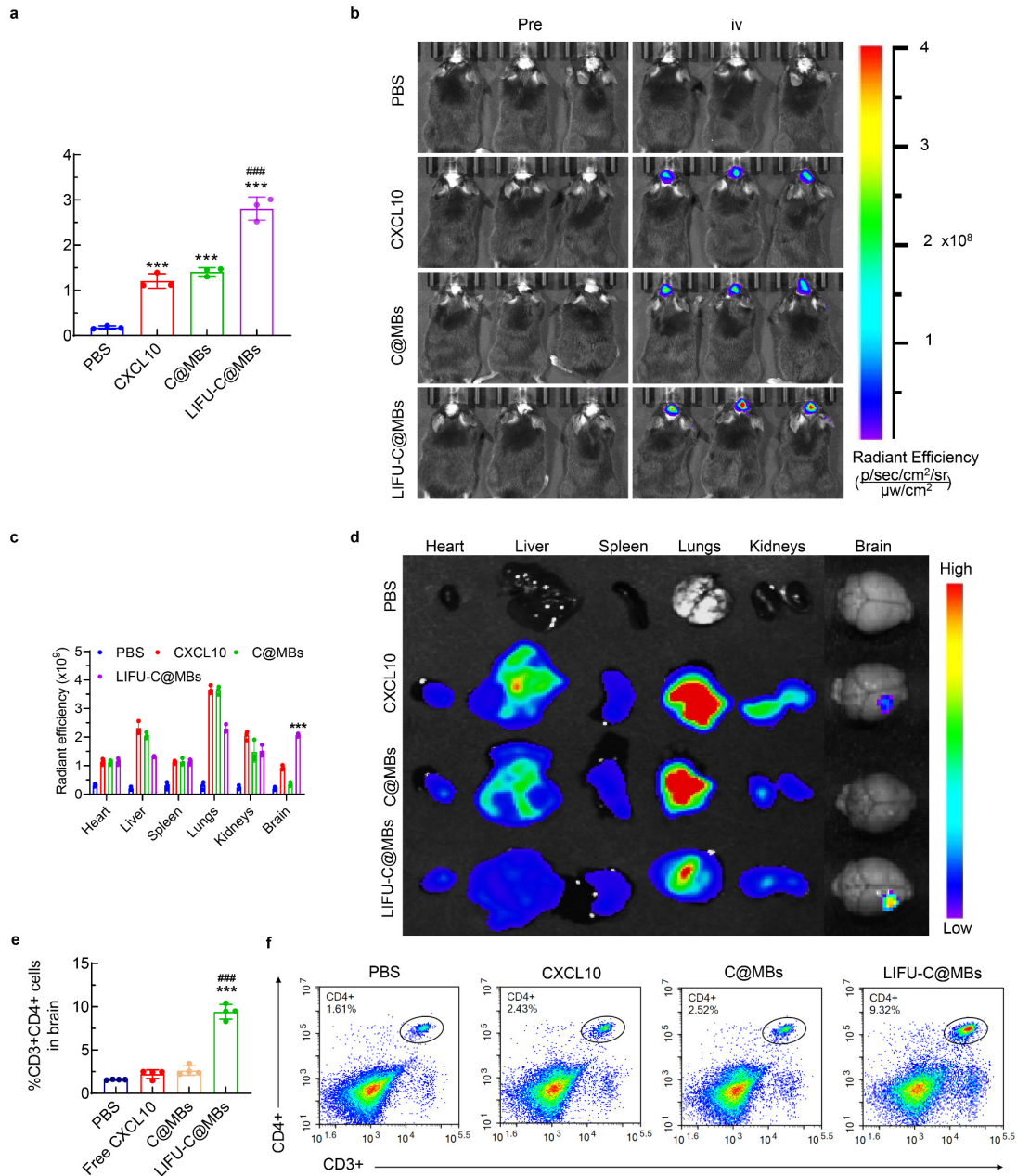


Figure S10. CXCL10 delivery efficiency and organ distribution of LIFU-conjugated C@MBs. a b) CXCL10 was labeled by Cy5, and normal mouse brain images were acquired by an *in vivo* imaging system before and after treatment with various CXCL10 preparations, respectively (n=3). c, d) Heart, liver, spleen, lung, kidney, and brain tumor distribution of CXCL10 was observed by *IVIS* (n=3). e, f) Ultrasound intensity was set at 0.40 w/cm² and flow quantification of the proportion of CD4⁺ T cells recruited after LIFU combined with C@MBs open BBB (n=4). Data are expressed as mean \pm standard deviation. Statistical significance was calculated by one-way ANOVA with the Tukey post hoc test. ****p* < 0.001, ###*p* < 0.001.

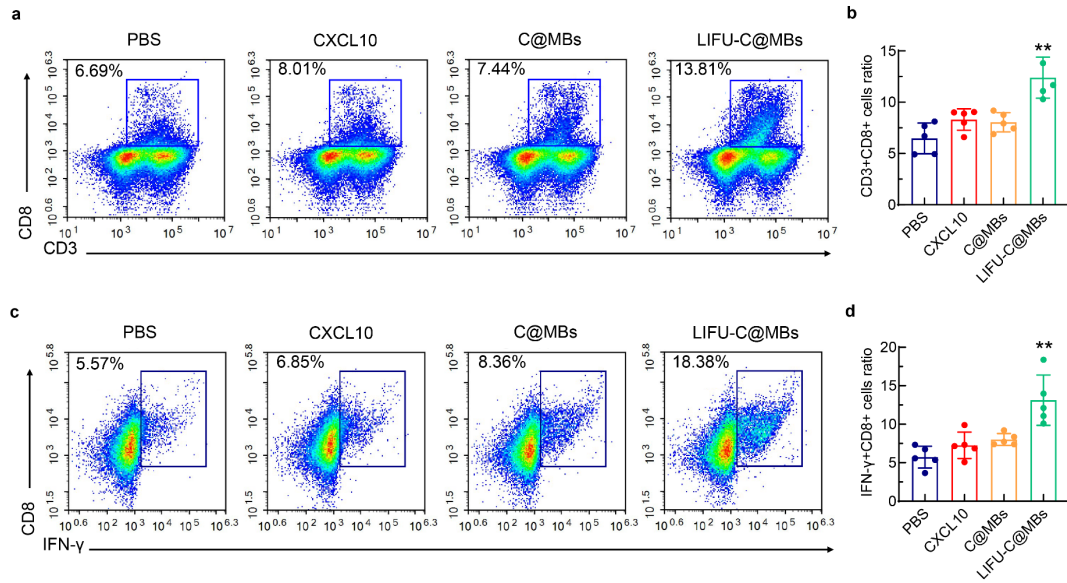


Figure S11. Proportion of tumor antigen-specific T cells. a, b) Proportion of tumor antigen-specific CD3⁺CD8⁺ T cells in tumor tissues by flow statistics (n=4). c, d) Proportion of tumor antigen-specific IFN-γ⁺CD8⁺ T cells in tumor tissues by flow statistics. Data are expressed as mean ± standard deviation. Statistical significance was calculated by one-way ANOVA with the Tukey post hoc test. ***p* < 0.01.

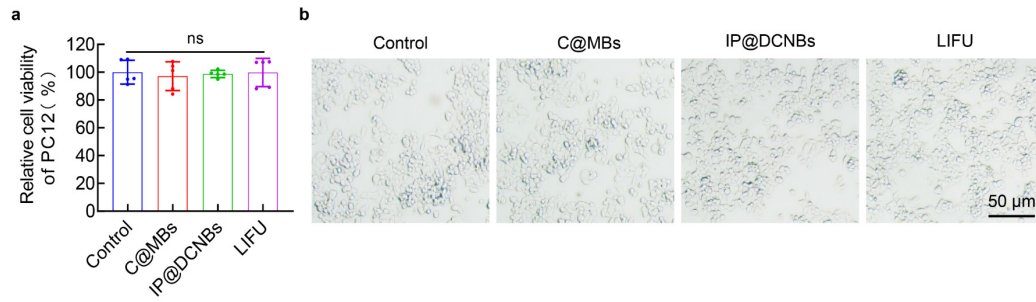


Figure S12. PC12 cell viability was determined by CCK-8 assay. C@MBs and IP@DCNBs were co-incubated with PC12 cells for 24h, respectively, and PC12 cells were treated with LIFU at sound intensities of 0.40 and 0.70 w/cm² (n=5). All statistics are expressed as mean ± standard deviation. Statistical significance was calculated by one-way ANOVA with the Tukey post hoc test. ns: no significance.

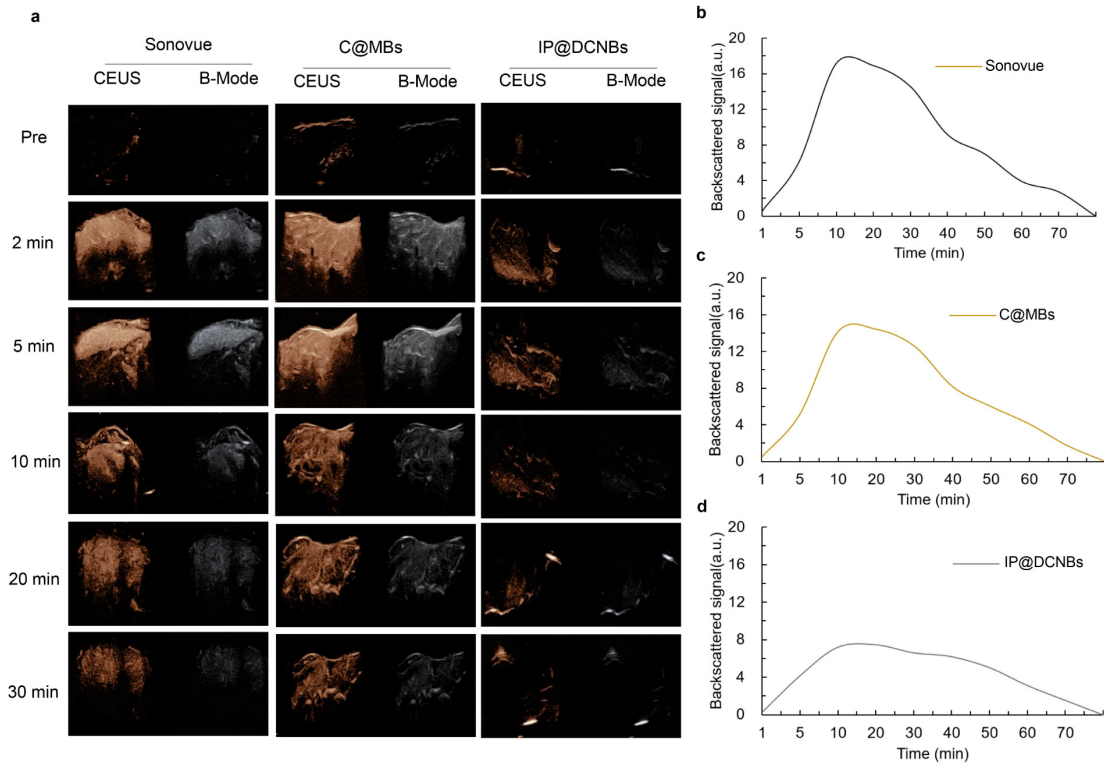


Figure S13. *In vivo* ultrasound imaging effects of Sonovue, C@MBs, and IP@DCNBs. The *in vivo* ultrasound imaging effect (liver, concentration of $1.4 \times 10^7/\text{mL}$ for all) was assessed by intravenous injection of $20 \mu\text{L}$ of Sonovue, C@MBs, and IP@DCNBs in CEUS and B-Mode modes of the ultrasound imaging system, which led to the determination of their *in vivo* stability. The *in vivo* stability of C@MBs was assessed in CEUS and B-Mode modes of the ultrasound imaging system (liver).

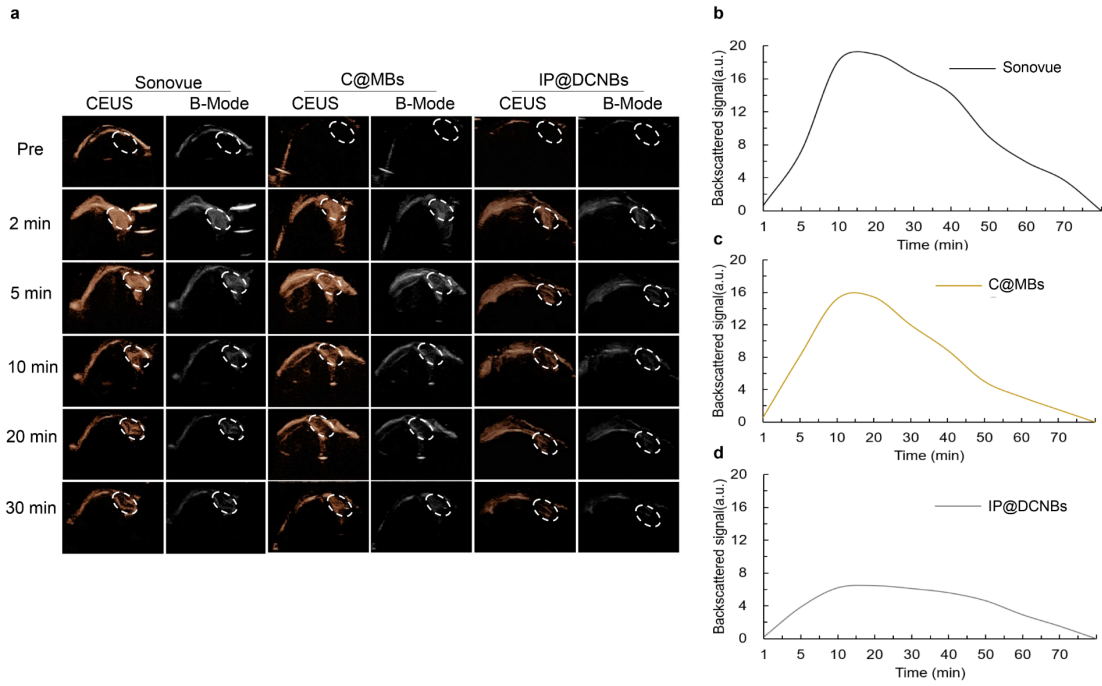


Figure S14. In situ ultrasound imaging effects of Sonovue, C@MBs, and IP@DCNBs in gliomas. The in situ ultrasound imaging effect of Sonovue, C@MBs, or IP@DCNBs in gliomas was evaluated by injecting 20 μL of Sonovue, C@MBs, or IP@DCNBs intravenously under CEUS and B-Mode modes of the ultrasound imaging system (all at a concentration of $1.4 \times 10^7/\text{mL}$).

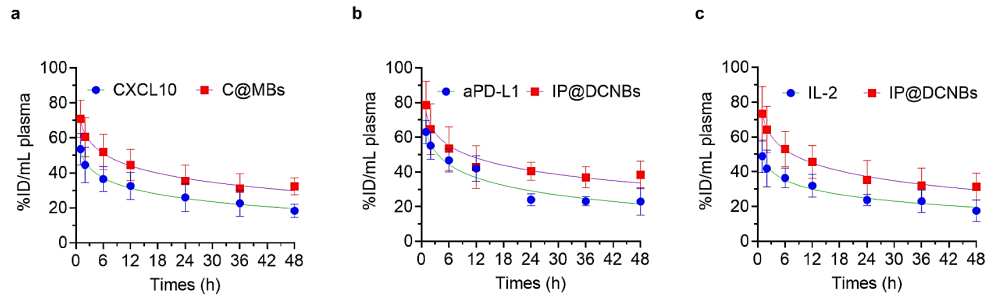


Figure S15. Blood circulation of various nanoformulations. *In vivo* pharmacokinetics of native CXCL10, aPD-L1, IL-2, C@MBs and IP@DCNBs (n = 3, aPD-L1 dose = 1.5 mg/kg, CXCL10 or IL-2 dose = 75 μ g/kg). Data are presented as means \pm SD.

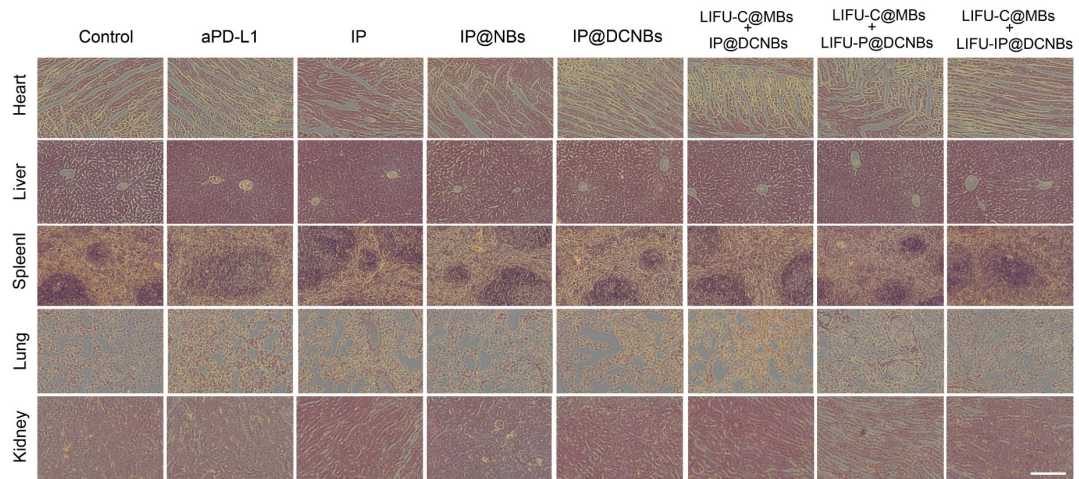


Figure S16. HE staining of heart, liver, spleen, lung, and kidney tissue sections was performed after various treatments. Seven days after injection of various nanopreparations, mice were euthanized and viscera (heart, liver, spleen, lungs, and kidneys) were excised, followed by HE staining to detect potential damage. Scale bar=50 μ m.

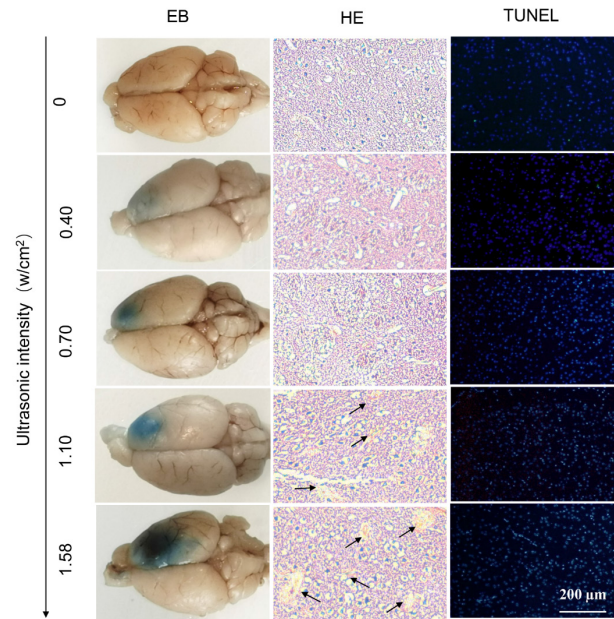


Figure S17. Safety of LIFU combined C@MBs open BBB. The open BBB region was subjected to section HE staining and TUNEL fluorescence apoptosis detection (LIFU combined with C@MBs treatment at sound intensities of 0.40, 0.70, 1.10, and 1.58 w/cm²).

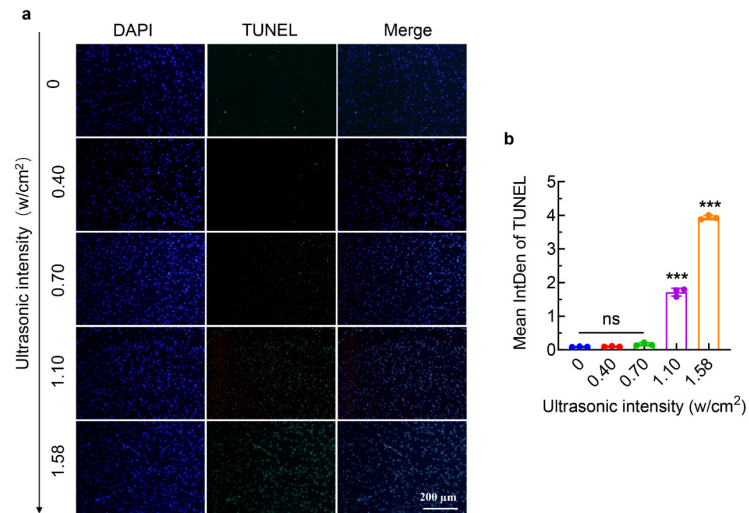


Figure S18. TUNEL apoptosis assay of the open region of the blood-brain barrier. ImageJ was performed to quantify the fluorescence signal (n=3). All statistics are expressed as mean \pm standard deviation. Statistical significance was calculated by one-way ANOVA with the Tukey post hoc test. *** $p < 0.001$, ns: no significance.

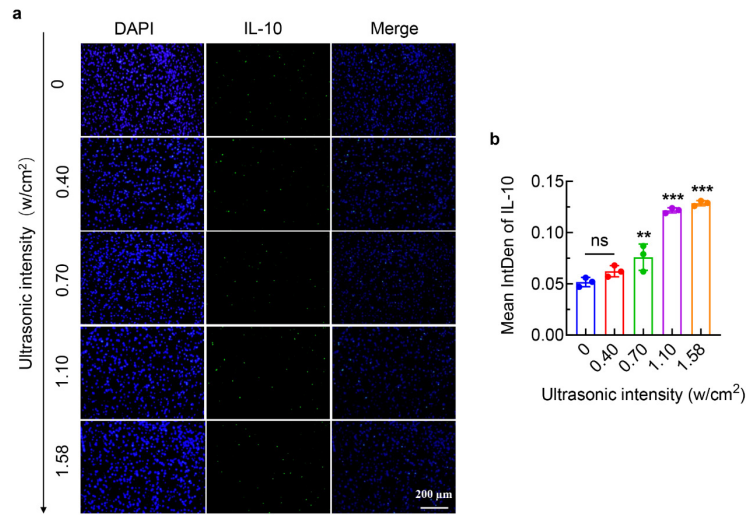


Figure S19. Inflammatory factor IL-10 levels in the open region of the blood-brain barrier. ImageJ was performed to quantify the fluorescence signal (n=3). All statistics are expressed as mean \pm standard deviation. Statistical significance was calculated by one-way ANOVA with the Tukey post hoc test. ** $p < 0.01$, *** $p < 0.001$, ns: no significance.

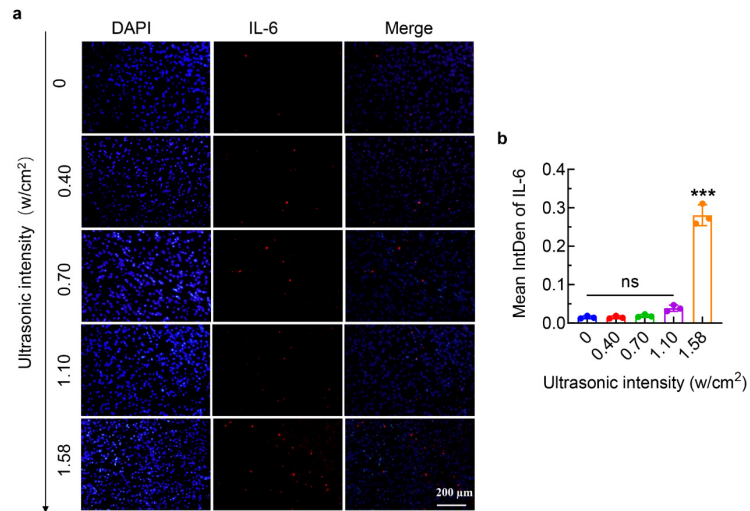


Figure S20. Inflammatory factor IL-6 levels in the open region of the blood-brain barrier. ImageJ was performed to quantify the fluorescence signal (n=3). All statistics are expressed as mean \pm standard deviation. Statistical significance was calculated by one-way ANOVA with the Tukey post hoc test. *** $p < 0.001$, ns: no significance.

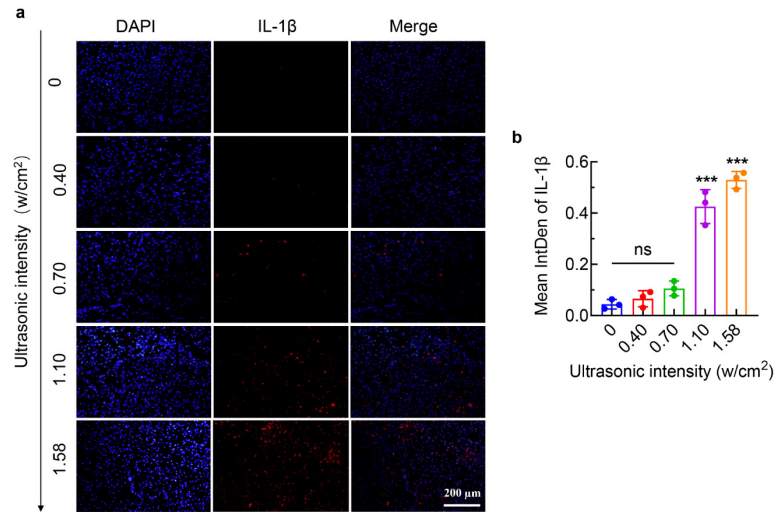


Figure S21. Inflammatory factor IL-1 β levels in the open region of the blood-brain barrier. ImageJ was performed to quantify the fluorescence signal (n=3). All statistics are expressed as mean \pm standard deviation. Statistical significance was calculated by one-way ANOVA with the Tukey post hoc test. *** $p < 0.001$, ns: no significance.

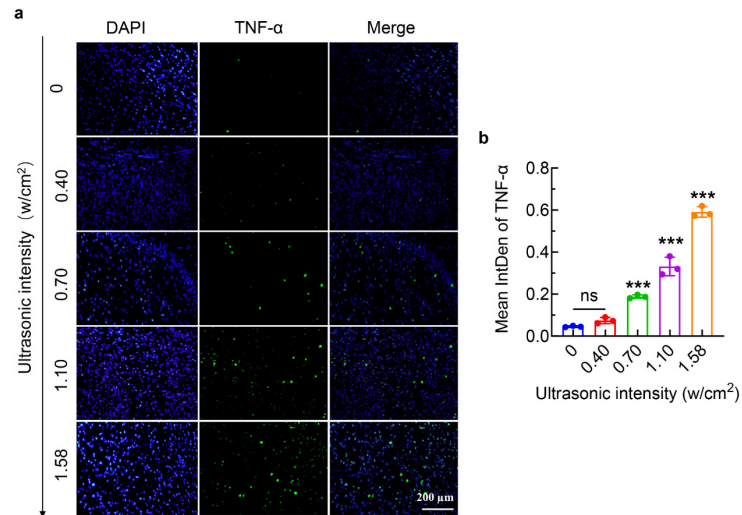


Figure S22. Inflammatory factor TNF- α levels in the open region of the blood-brain barrier. ImageJ was performed to quantify the fluorescence signal (n=3). All statistics are expressed as mean \pm standard deviation. Statistical significance was calculated by one-way ANOVA with the Tukey post hoc test. *** $p < 0.001$, ns: no significance.

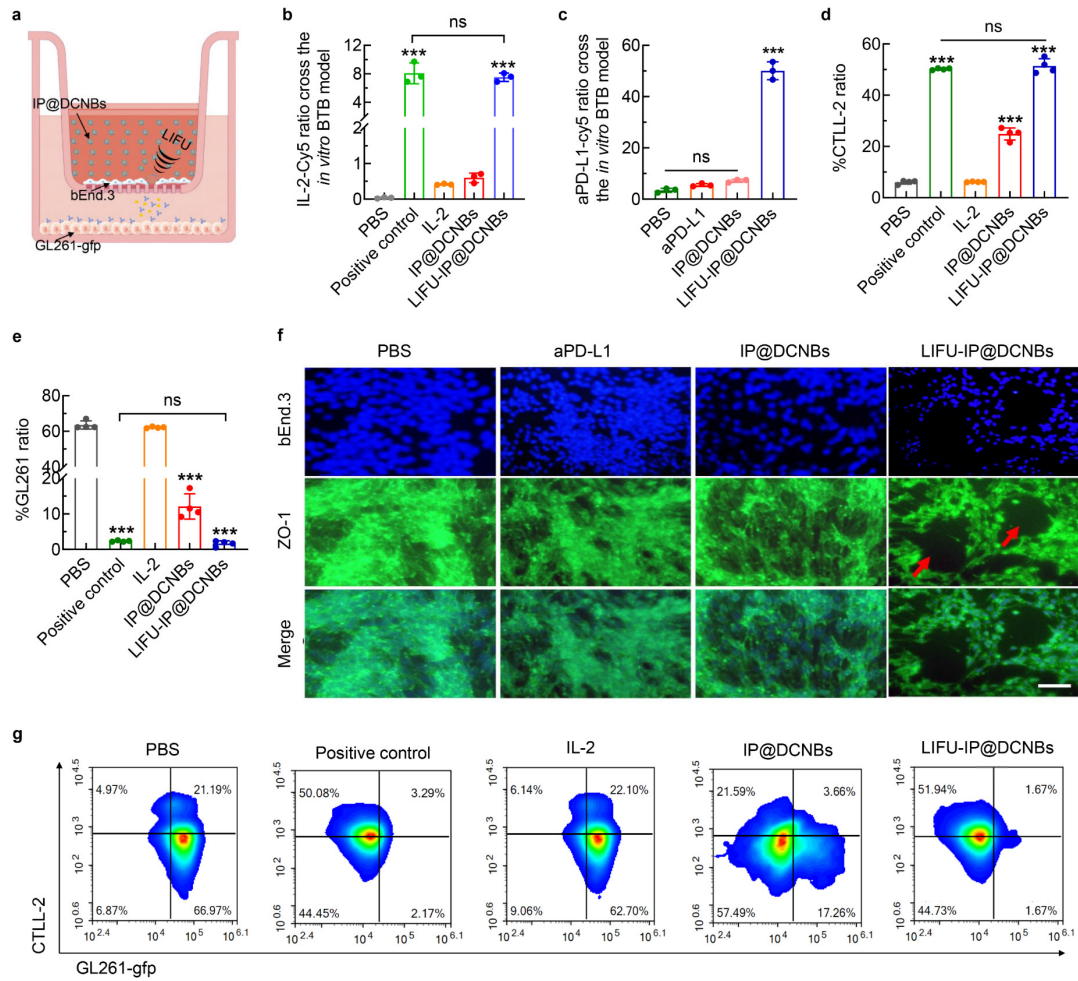


Figure S23. Delivery efficiency assessment of IP@DCNBs. aPD-L1 delivery efficiency by LIFU combined with IP@DCNBs. a) Schematic diagram of the *in vitro* BTB model used for delivery capacity assessment. b, c) Multi-functional zymography for quantification of IL-2 and aPD-L1 in the lower compartment (n=3). d, e, g) Relative cell viability of lower compartment T-cells and GL261 cells after treatment with different IL-2 preparations as measured by CCK-8 assay and flow cytometry (n=4). f) Fluorescence microscopy observation of bEnd.3 cells opening of the constructed BTB model (fluorescent secondary antibody goat anti-rabbit IgG H&L (Alexa Fluor® 647) labeled with tight junction protein ZO-1). Scale bar=50μm. Data are expressed as mean ± standard deviation. Statistical significance was calculated by one-way ANOVA with the Tukey post hoc test. ****p* < 0.001, ns: no significance.

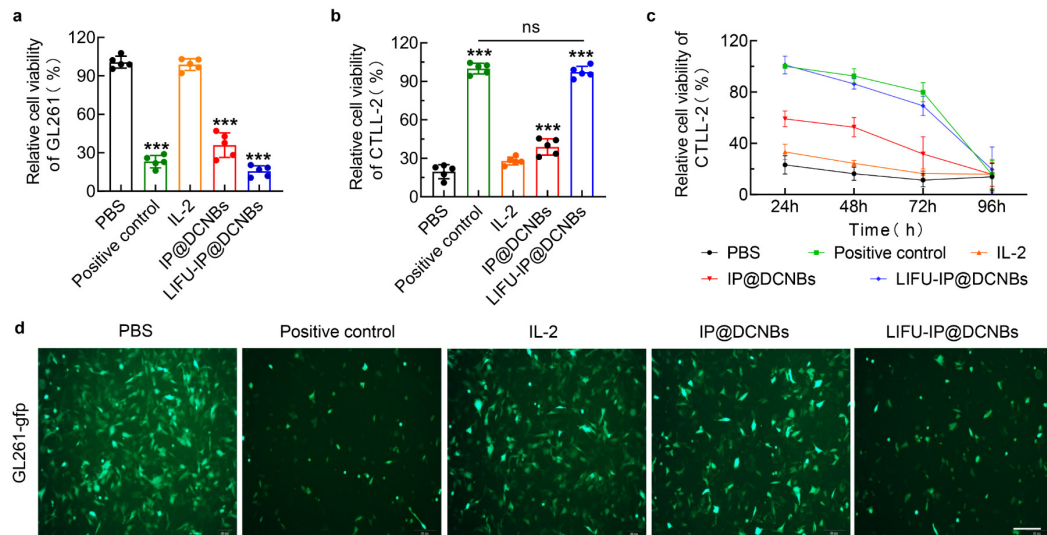


Figure S24. LIFU combined with IP@DCNBs results in reduced CTLL-2 cell exhaustion. a, b) Flow-quantification and cell viability of lower compartment T-cells and GL261 cells after treatment with different IL-2 preparations (n=5). c) CTLL-2 cell viability corresponding to different time points (n=5). d) The viability of GL261 cells in the lower compartment was observed by fluorescence microscopy. Scale bar=50 μ m. Data are expressed as mean \pm standard deviation. Statistical significance was calculated by one-way ANOVA with the Tukey post hoc test. *** $p < 0.001$, ns: no significance.

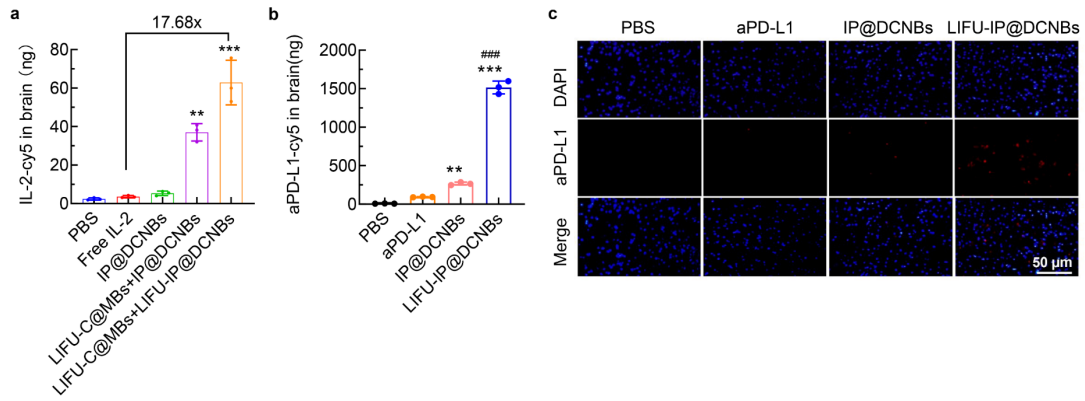


Figure S25. LIFU combined with IP@DCNBs open BTB modeling. a) Delivery efficiency of IL-2-cy5 in GBM was assessed by enzyme markers (n=3 bio-independent samples). b) Quantification of aPD-L1 in brain tissues by multifunctional enzyme marker (n=3 bio-independent samples). c) Observation of the distribution of aPD-L1 in the GBM by brain tumor tissue sectioning. Data were expressed as mean \pm standard deviation. Statistical significance was calculated by one-way ANOVA with Tukey's post hoc test. $**p < 0.01$, $***p < 0.001$, and $###p < 0.001$, ns: no significance.

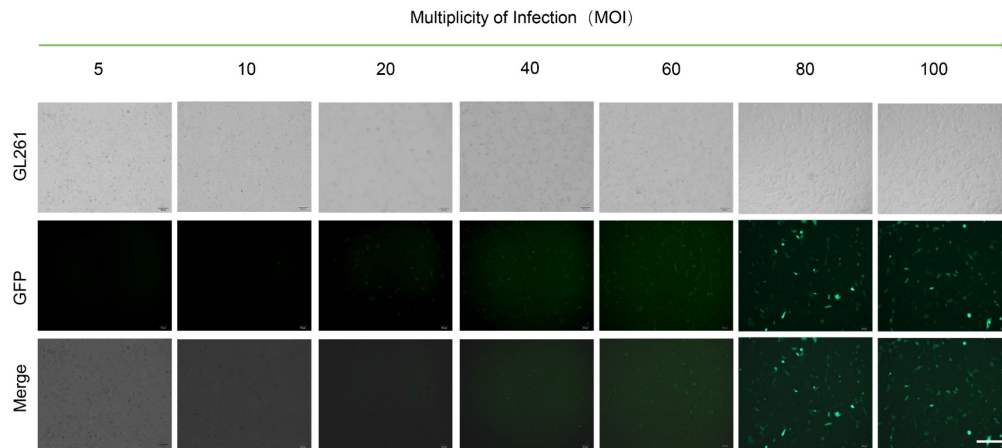


Figure S26. Lentiviral transfection to construct GL261-GFP-Luc cells. Fluorescence images of GFP-luc-puro lentivirus transfected GL261 cells 72h after different MOI values were observed by fluorescence microscopy. Scale bar=50 μ m.

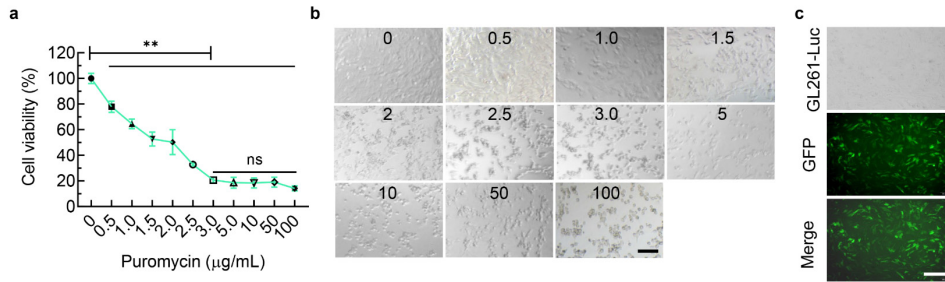


Figure S27. Screening of stable GL261-GFP-Luc cells with puromycin. a, b) CCK-8 assay to detect the effect of different concentrations of puromycin on the viability of GL261 cells, and light microscopy to observe the cell viability (n=3). Scale bar=50μm. c) Fluorescence microscopy to observe the expression of GFP in the screened GL261-Luc cell line (puromycin concentration of 3μg/mL). d) Fluorescence microscopy to observe the expression of GFP in the screened GL261-Luc cell line (puromycin concentration of 3μg/mL). Scale bar=50μm. All statistics are expressed as mean ± standard deviation. Statistical significance was calculated by one-way ANOVA with the Tukey post hoc test. ** $p < 0.01$.

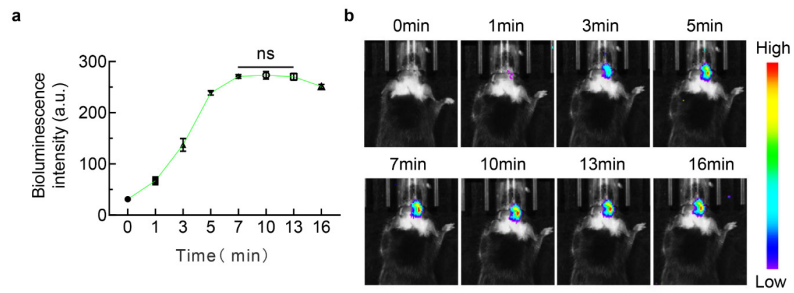


Figure S28. Stabilized detection of time-slotted *in vivo* imaging systems. The *in vivo* imaging system detected the fluorescence signal of the dual fluorescein-labeled GBM in situ mouse model at various periods (intraperitoneal injection of D-fluorescein potassium salt at 150 mg/kg, n=3). All statistics are expressed as mean \pm standard deviation. Statistical significance was calculated by one-way ANOVA with the Tukey post hoc test. ns: no significance.

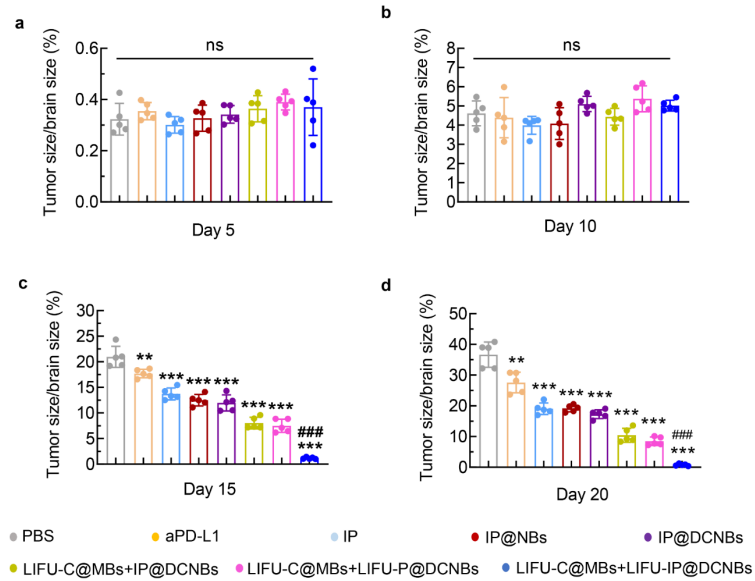


Figure S29. Tumor size detection by MRI. The anti-tumor efficacy of various treatments was assessed by MRI system (T2 MRI) on days 5, 10, 15, and 20 of constructing the dual fluorescein-labeled GBM in situ mouse model, and the tumor-to-brain area ratio was calculated by ImageJ (n=5). All statistics are expressed as mean \pm standard deviation. Statistical significance was calculated by one-way ANOVA with the Tukey post hoc test. ** $p < 0.01$, *** $p < 0.001$, and ### $p < 0.001$, ns: no significance.

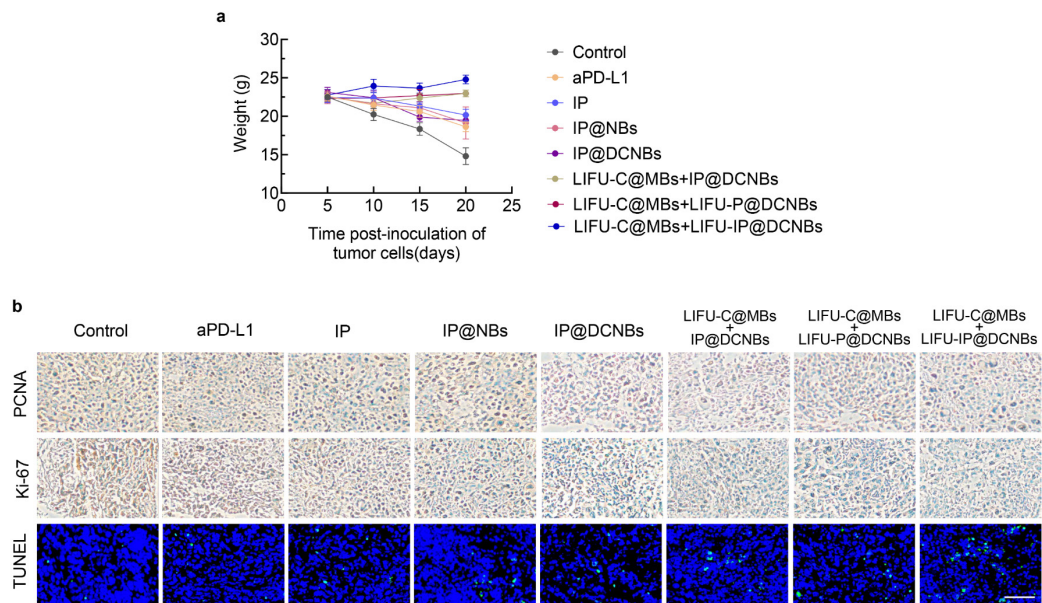


Figure S30. Weight monitoring of GL261 in situ GBM mice. a) Mice in each treatment group were weighed on days 5, 10, 15, and 20 of constructing the GL261 in situ GBM mouse model (n=5). b) Immunohistochemical images of tumor sections were examined at 20 days of rhabdomyolysis (Ki-67, PCNA, and TUNEL). Scale bar=50 μ m.

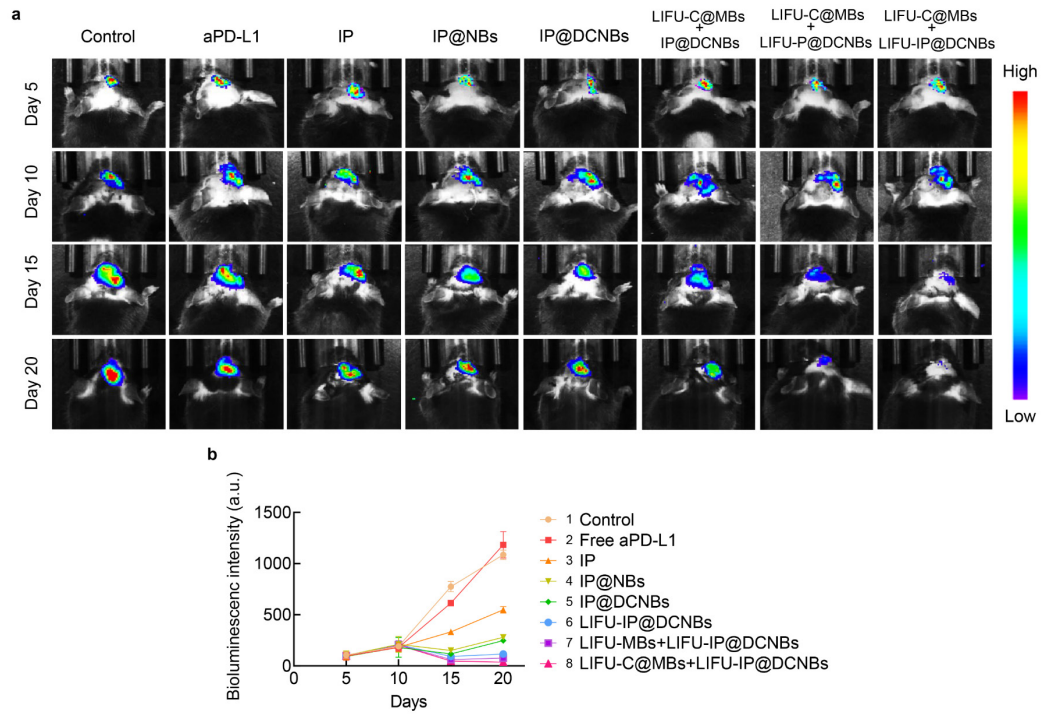


Figure S31. *In vivo* imaging system to assess anti-tumor efficacy. Antitumor efficacy of various treatments was assessed by an *in vivo* imaging system on days 5, 10, 15, and 20 of constructing the dual fluorescein-labeled *in situ* mouse model of GBM (n=5).

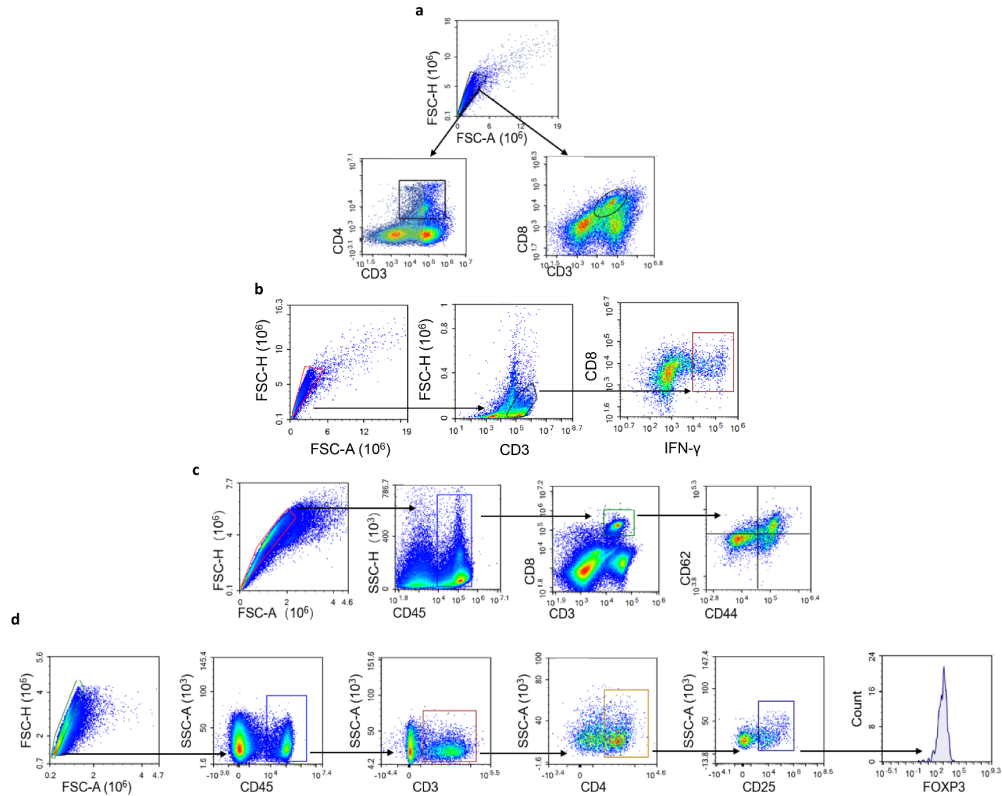


Figure S32. Graphical illustration of flow cytometry gating strategies for CD8⁺ T cells, memory T cells, and Treg cells. a) Gating strategy for sorting CD8⁺ T cells on CD3⁺ cells in tumor tissues versus CD4⁺ T cells. b) Gating strategy for sorting IFN-γ⁺ CD8⁺ Tumor antigen-specific T cells on CD3⁺ cells in tumor tissues. c) Gating strategy for sorting CD62L⁻ CD44⁺ effector memory T cells (TEM) on CD3⁺ CD8⁺ cells in splenic tissues versus CD62L⁺ CD44⁺ central memory T cells (TCM). d) Gating strategy for sorting Foxp3⁺ Treg cells in tumor tissues gated on CD4⁺ cells.

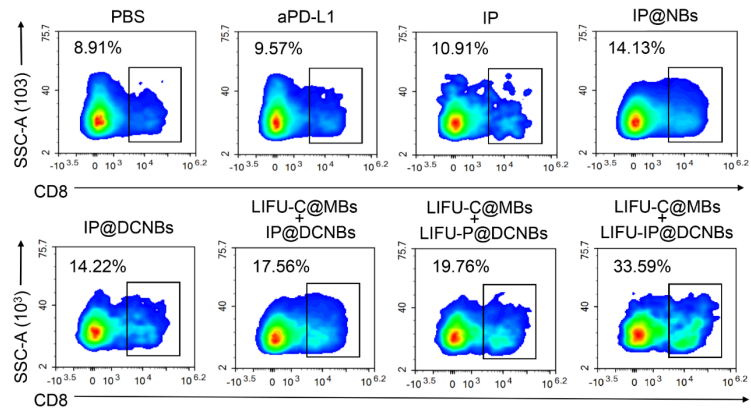


Figure S33. CD8⁺ T cells in tumor tissue. The proportion of CD8⁺ T cells in tumor tissues was detected by flow cytometry on day 17 of the construction of the GL261 in situ GBM mouse model.

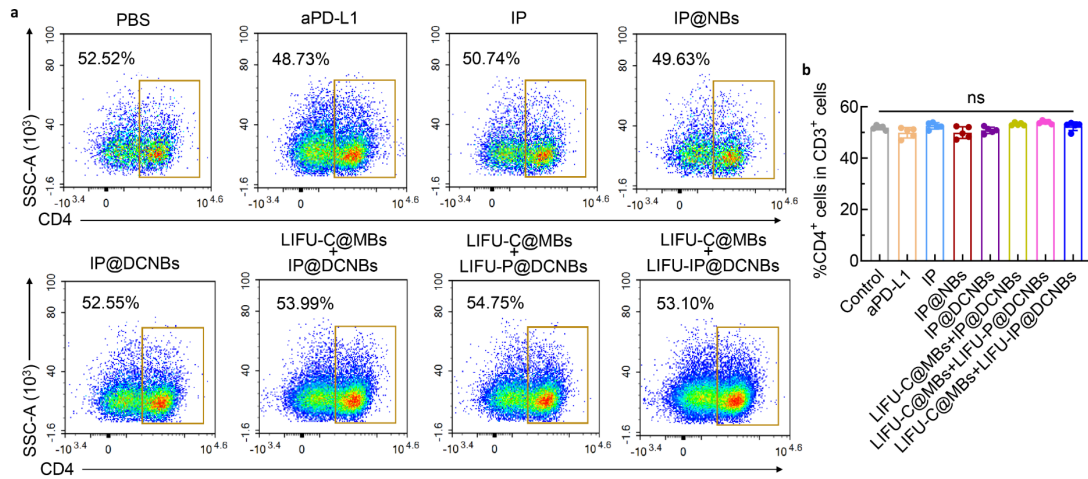


Figure S34. CD4⁺ T cells in tumor tissue. The proportion of CD4⁺ T cells in tumor tissues was examined by flow cytometry on day 17 of the construction of the GL261 in situ GBM mouse model (n=5). All statistics are expressed as mean ± standard deviation. Statistical significance was calculated by one-way ANOVA with the Tukey post hoc test. ns: no significance.

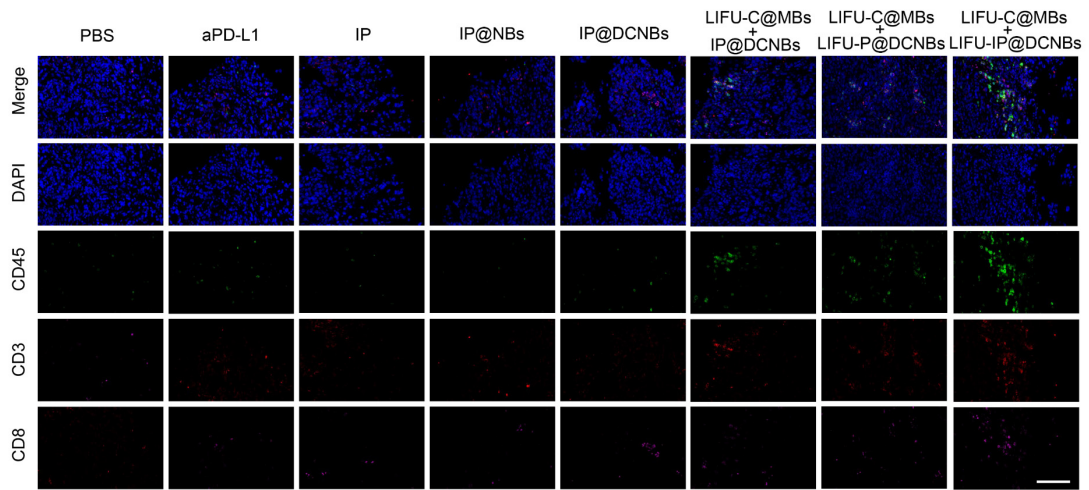


Figure S35. Representative immunofluorescence images of tumor-infiltrating CD8⁺ T cells.
Scale bar=50 μ m.

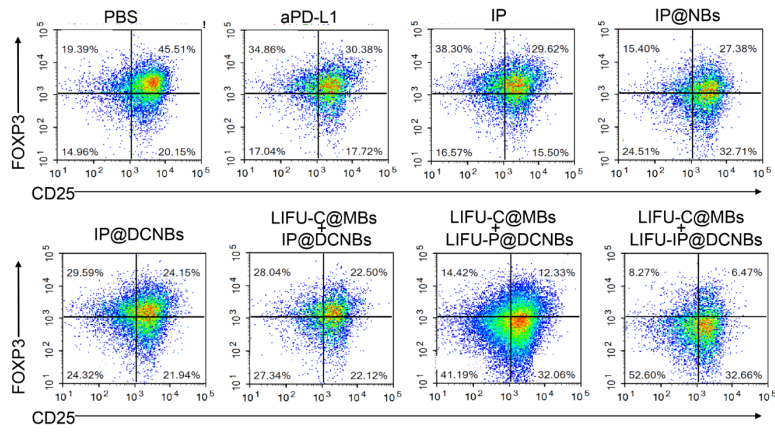


Figure S36. Treg cell proportion in tumor tissues. The proportion of Treg cells in tumor tissues was detected by flow cytometry on day 17 of the construction of the GL261 in situ GBM mouse model.

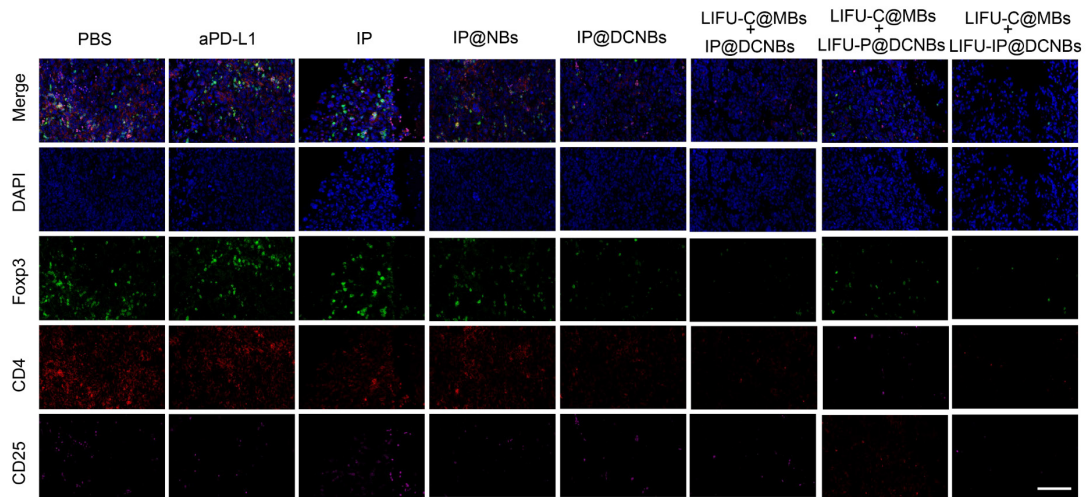


Figure S37. Representative immunofluorescence images of tumor-infiltrating Treg cells.
Scale bar=50 μ m.

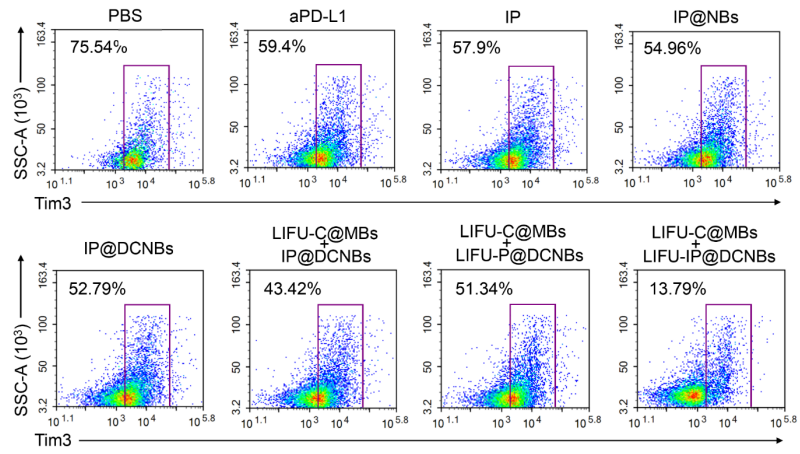


Figure S38. Tim3 expression of CD8⁺ T cell. The proportion of CD8⁺ T cells expressing Tim3 in tumor tissues was detected by flow cytometry on day 25 of constructing the GL261 in situ GBM mouse model.

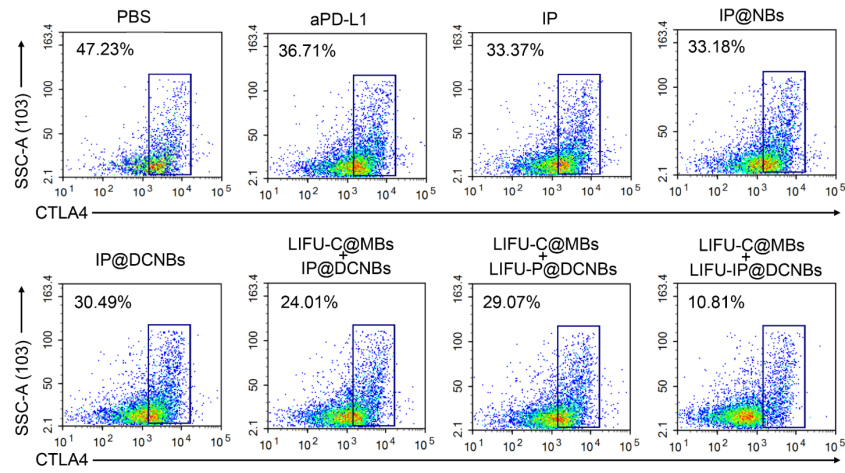


Figure S39. CTLA4 expression of CD8⁺ T cell. The proportion of CD8⁺ T cells expressing CTLA4 in tumor tissues was detected by flow cytometry on day 25 of constructing the GL261 in situ GBM mouse model.

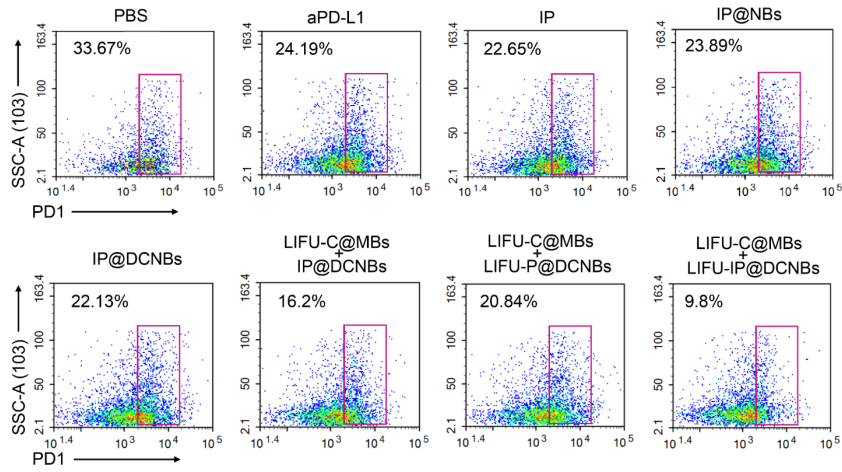


Figure S40. PD1 expression of CD8⁺ T cell. The proportion of CD8⁺ T cells expressing PD1 in tumor tissues was detected by flow cytometry on day 25 of constructing the GL261 in situ GBM mouse model.

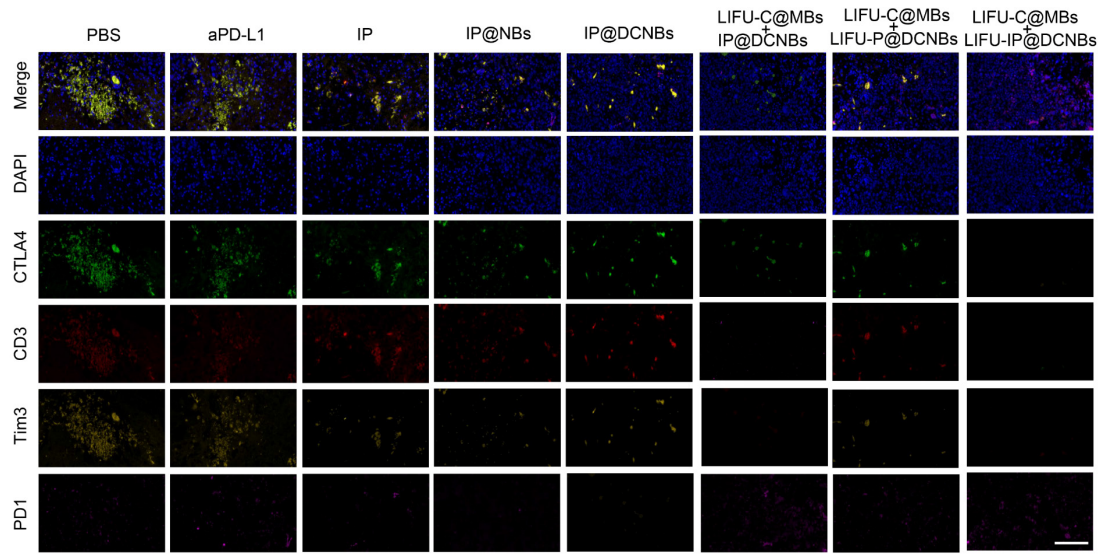


Figure S41. Representative immunofluorescence images of tumor-infiltrating exhausted CD8⁺ T cells. Scale bar=50 μ m.

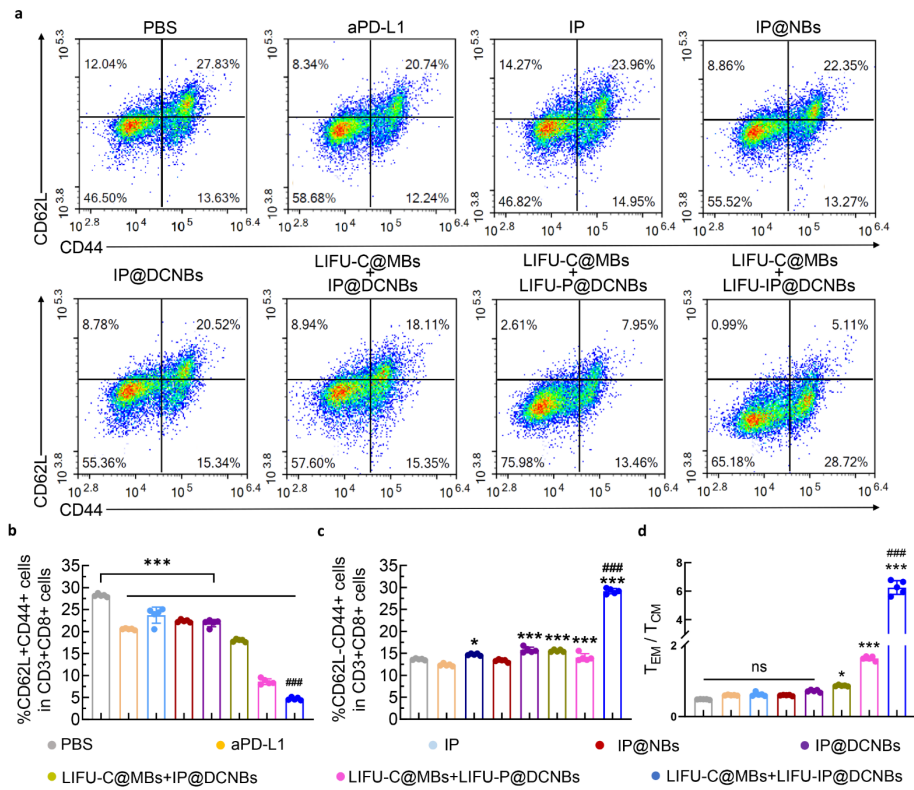


Figure S42. Detection of memory T cells in tumor tissue. a, b, c, d) On day 25 of constructing the GL261 in situ GBM mouse model, the proportions of CD62L⁺CD44⁺ effector memory T cells (TEM) and CD62L⁺CD44⁺ central memory T cells (TCM) on CD3⁺CD8⁺ cells were examined by flow cytometry in spleen tissues of in situ GBM mice (n=5). All statistics are expressed as mean ± standard deviation. Statistical significance was calculated by one-way ANOVA with the Tukey post hoc test. **p* < 0.05, ****p* < 0.001, and ###*p* < 0.001, ns: no significance.

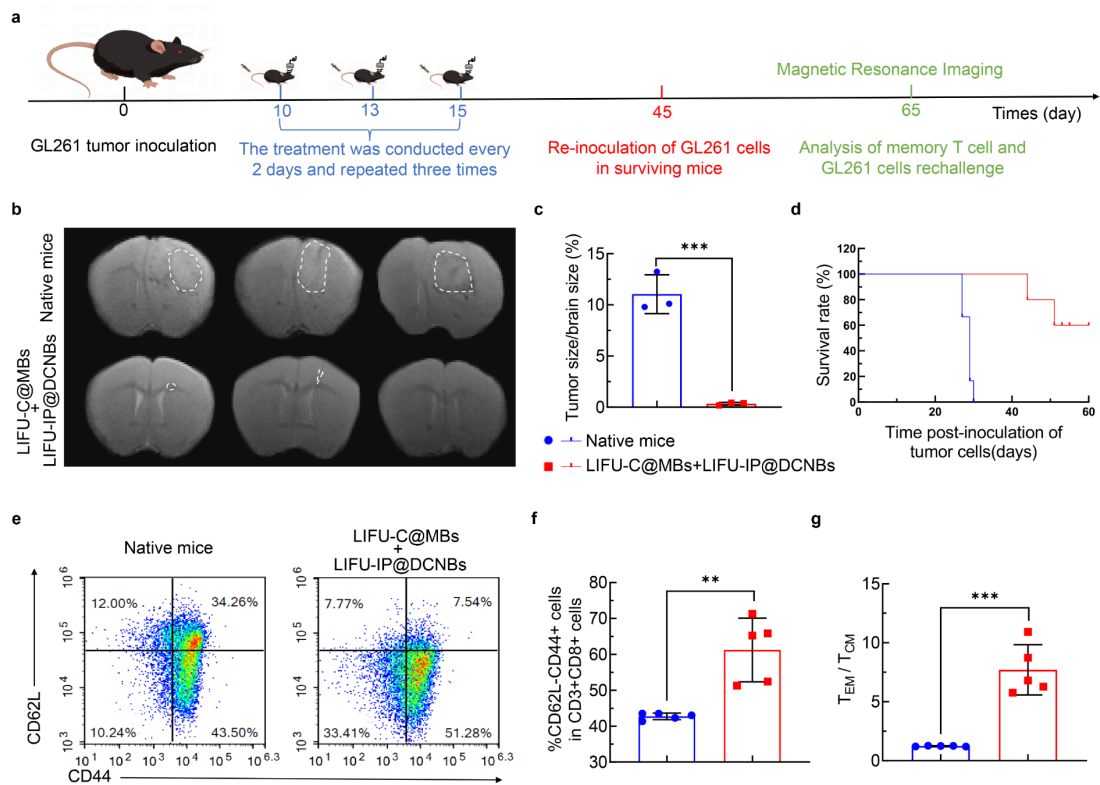


Figure S43. Tumor re-implantation and long-term immune memory. a) Treatment schedule of GL261 mouse brain tumor model. b, c, d) T2-weighted images and quantitative analysis data of natural and LIFU-C@MBs+LIFU-IP@DCNBs-treated mice 20 days after reimplantation. For tumor re-excitation experiments, mice were inoculated with 1×10^5 GL261 tumor cells to the opposite (left) side. Native mice were used as controls. b, Survival curves of natural and A2-MPC-treated mice after re-excitation with GL261 cells. e, f, g) Quantification of CD62L⁻CD44⁺ effector memory T cells (T_{EM}) and the ratio of T_{EM} to CD62L⁺CD44⁺ central memory (T_{CM}) in the spleens of natural mice and LIFU-C@MBs + LIFU-IP@DCNBs treated mice by FACS. All statistics are expressed as mean \pm standard deviation. Statistical significance was calculated by one-way ANOVA with the Tukey post hoc test. ** $p < 0.01$, *** $p < 0.001$.